Electromagnetic Properties of Pseudoscalar Mesons via the Primakoff Effect at 11 GeV

The PrimEx Collaboration

Contributing Editors:

A. Gasparian
North Carolina A&T State University

L. Gan
University of North Carolina at Wilmington

J. Goity
Hampton University

D. Dale
University of Kentucky

A. Bernstein
Massachusetts Institute of Technology

R. Miskimen
University of Massachussetts

December 2, 2002

Contents

1 Abstract

We propose to extend our precision measurement of the $\pi^0 \rightarrow \gamma\gamma$ decay width via the Primakoff effect to include the η and $\eta^{'}$ mesons. We also propose to measure the transition form factors of all of the pseudoscalar mesons (π^o, η, η'). This will become possible with the advent of a 12 GeV electron beam at Jefferson Lab. These precision measurements would have a significant impact in the experimental determination of the ratios of the light quark masses (m_u, m_d, m_s), and on our understanding of some fundamental issues in QCD. They will provide tests of both QCD and QCD based models, including the magnitude of $\eta, \eta^{'}$ mixing. At a more general level, these measurements impact the issue of spontaneous chiral symnmetry breaking in QCD, and the intriguing question of whether the $\eta^{'}$ meson can be considered as an approximate Goldstone Boson in the combined chiral and large N_c expansions. The proposed measurements of the π^o, η and η' transition form factors at very low Q^2 (~ 0.001–$0.5 GeV^2$) would provide a first measurement of these important quantities. The slopes of the transition form factors approximately measure the spatial distribution of the axial anomaly. The η' form factor slope tests the U(3) flavor symmetry implied by the large N_c limit. In this limit, the same low energy term determines all three transition form factor slopes. The proposed instrumentation to be constructed for this program will be of general utility for both this program and future experiments, and will provide a new and powerful experimental window on QCD at JLab in an arena where the basic theory is well established. In addition, the important contribution of the transition form factors of the pseudoscalar mesons to the muon anomalous magnetic moment is discussed. These measurements are thus important for the search for "new physics" beyond the Standard Model.

2 Introduction

The future availability of high quality, high duty factor 11 GeV electron beams at JLab will enable unprecedented new opportunities to perform precise measurements of meson decay widths and electromagnetic transition form factors. Here, we detail how one can exploit the high energy electro- and photoproduction of pseudoscalar mesons in the Coulomb field of a nucleus, the so called Primakoff effect, to study the two photon decay widths, $\Gamma_{\gamma\gamma}$, and the transition form factors, $F_{\gamma\gamma^* P}$, where P represents the π^o, η, and η' pseudoscalar mesons. This comprehensive program will provide fundamental tests of both quantum chromodynamics and QCD inspired models.

This represents an update of a proposal presented to PAC18. In their report [1], it was mentioned as one of "two experiments reviewed by the committee (that would) definitely require higher energy beams and did resonate with the PAC members." Furthermore, the report "strongly encourages work to assure the feasibility of this promising program." This update describes progress made since PAC18 on the development of the experimental setup as well as on the theoretical front. In addition to the proposed 11 GeV upgrade to the CEBAF accelerator, this program will require: (1) a high energy photon tagging facility, and (2), an upgraded PrimEx calorimeter for detection of multiphoton states as well as scattered electrons. The requirements for this instrumentation and the physics which it will make possible are described below.

3 Motivation

The three neutral pseudoscalar mesons, the π^0, η and the η', represent one of the most interesting systems in strong interactions. This system contains fundamental information about the effects of SU(3) and isospin breaking by the u, d, and s quark masses, leading to important mixing effects among the mesons. In addition, it shows the effects of two types of chiral anomalies, namely, the $U_A(1)$ anomaly that involves the flavor singlet axial current $j^\mu_A = \bar{q}\gamma^\mu\gamma_5 q$ and the color currents, and the anomalies involving either the singlet axial current or one of the two neutral axial currents ($j^\mu_{A3} = \bar{q}\gamma^\mu\gamma_5\lambda_3 q$ and $j^\mu_{A8} = \bar{q}\gamma^\mu\gamma_5\lambda_8 q$, where $q = (u, d, s)^T$) and two electromagnetic currents. The first anomaly is responsible for much of the η' mass, while the latter drives the two-photon decays of these mesons.

The QCD Lagrangian,

$$\mathcal{L}_{QCD} = \sum_{i=u,d,s} \bar{\psi}_i (i \not{\partial} - g \not{G} - m_i)\psi_i - \frac{1}{4} G^a_{\mu\nu} G^{\mu\nu}_a, \tag{1}$$

is invariant under an enlarged group of flavor symmetry transformations in the limit of massless quarks (chiral limit). This group is the chiral $SU_L(3) \times SU_R(3) \times U_A(1) \times U_{baryon}(1)$. As a consequence of these symmetries, the Noether currents associated with infinitesimal axial transformations are conserved in the classical theory. These two symmetries are realized differently in the full quantum field theory. Chiral $SU_L(3) \times SU_R(3)$ is not only a symmetry of the classical QCD Lagrangian, but also a symmetry of the full quantum field theory. The

$U_A(1)$ symmetry, however, is broken explicitly by the so called axial anomaly that induces a non-conservation of the associated Noether current. Thus in the full quantum theory and in the chiral limit, QCD has the symmetry $SU_L(3) \times SU_R(3) \times U_{baryon}(1)$. The condensation of quark-anti-quark pairs in the QCD vacuum gives rise to a phenomenon of spontaneous breaking of this chiral symmetry down to the flavor $SU(3)$ symmetry that is the symmetry of the vacuum. As a result, there are eight massless Goldstone Bosons corresponding to the eight spontaneously broken symmetry generators. The eight Goldstone Bosons are identified with the octet of pseudoscalar mesons (π^0, $\pi^{\pm}$, $K^{\pm}$, K^0, $\bar{K}^0$, and η). In reality, the quark masses are non zero (albeit small), thus breaking the chiral symmetry explicitly and giving rise to masses for the Goldstone Bosons following the mechanism discovered by Gell-Mann, Oakes and Renner [2].

As mentioned above, the axial $U_A(1)$, unlike chiral $SU_L(3) \times SU_R(3)$, is no longer a symmetry of the full quantum theory, even though it is a symmetry of the classical QCD Lagrangian. The reason is because the $U_A(1)$ Noether current has a non-vanishing divergence known as the Adler-Bell-Jackiw anomaly or axial anomaly:

$$\partial_\mu j^\mu_A \mid_{Axial\ \ Anomaly} = \frac{N_F \alpha_s}{8\pi} \varepsilon^{\mu\nu\lambda\sigma} G^a_{\mu\nu} G_{a\lambda\sigma} \tag{2}$$

where $N_F = 3$ is the number of flavors appearing in the axial current, and G is the gluon field. The $U_A(1)$ symmetry is explicitly broken by the quantum fluctuations of the quark fields coupling to the gluon field, representing one of the most profound symmetry breaking phenomena in Nature. A consequence of the anomaly is that the η' meson in the chiral limit is no longer a Goldstone Boson associated with the spontaneous breaking of the $U_A(1)$ because it acquires a non-vanishing mass due to the axial anomaly. It is however important to note that in a certain limit in QCD the η' does become a Goldstone Boson. This is the limit in which the number of colors, N_c, is large. In this limit the axial anomaly, which is proportional to $\alpha_s \sim 1/N_c$, vanishes. As highlighted below, this limit has been recently exploited to build a highly predictive theoretical framework for studying the η'.

There is a second type of anomaly that involves the coupling of the quarks to the electromagnetic field. This leads to a similar non-vanishing divergence of the axial currents:

$$\begin{aligned}
\partial_\mu j^\mu_{A3} \mid_{EM\ \ Anomaly} &= \frac{N_c \alpha_{em}}{3\pi} \epsilon^{\mu\nu\rho\sigma} F_{\mu\nu} F_{\rho\sigma} \\
\partial_\mu j^\mu_{A8} \mid_{EM\ \ Anomaly} &= \frac{1}{\sqrt{3}} \frac{\alpha_{em}}{3\pi} \epsilon^{\mu\nu\rho\sigma} F_{\mu\nu} F_{\rho\sigma} \\
\partial_\mu j^\mu_{A} \mid_{EM\ \ Anomaly} &= \sqrt{\frac{3}{8}} \frac{N_c \alpha_{em}}{3\pi} \epsilon^{\mu\nu\rho\sigma} F_{\mu\nu} F_{\rho\sigma}
\end{aligned} \tag{3}$$

where the $F's$ are the electromagnetic fields, and N_c is the number of colors. This anomaly plays a crucial role in the physics of the (π^0, η, η') complex, being directly responsible for the

decays of the three mesons into photon pairs. In the chiral limit, the second type of anomaly leads to a rigorous prediction of the π^0, η and η' decay amplitudes into two photons:

$$A(\pi^o \to \gamma\gamma) = A_{\pi^0\gamma\gamma}\epsilon^{\mu\nu\rho\sigma}\epsilon_\mu\epsilon'_\nu k_\rho k'_\sigma$$

$$A(\eta_8 \to \gamma\gamma) = A_{\eta_8\gamma\gamma}\epsilon^{\mu\nu\rho\sigma}\epsilon_\mu\epsilon'_\nu k_\rho k'_\sigma$$

$$A(\eta_0 \to \gamma\gamma) = A_{\eta_0\gamma\gamma}\epsilon^{\mu\nu\rho\sigma}\epsilon_\mu\epsilon'_\nu k_\rho k'\sigma, \tag{4}$$

where ϵ and k represent photon polarizations and momenta respectively, and $A_{\pi^o\gamma\gamma} = -i\frac{\alpha_{em}}{8\pi F_\pi}$, $A_{\eta_8\gamma\gamma} = -i\frac{\alpha_{em}}{8\sqrt{3}\pi F_{\eta_8}}$, and $A_{\eta_0\gamma\gamma} = -i\frac{\alpha_{em}}{\sqrt{24}\pi F_{\eta_0}}$. The F's are the corresponding meson decay constants. While in the chiral limit SU(3) symmetry implies that $F_\pi = F_{\eta_8}$, F_{η_0} is not constrained by symmetries. However, in the limit of large number of colors (large N_c limit), one has $F_{\eta_0} = F_\pi$. Thus, in the chiral and large N_c limits the two-photon decays can be predicted. The important question is then what are the effects of the quark masses and the corrections due to the fact that $N_c = 3$.

Indeed, the relatively straightforward situation of the chiral limit becomes much more complex in the real world in which the quark masses are non-vanishing. In the real world the current quark masses are estimated to be $m_u \sim m_d/2 \sim 5$ MeV and $m_s \sim 150$ MeV at the renormalization QCD scale of about 1 GeV. These masses make the π^0 and the η massive and shift the mass of the η' due to explicit breaking of chiral symmetry, while SU(3) and isospin breaking induce mixings among the three mesons. The mixings are expressed in terms of three mixing angles [3]. Writing the eigenstates in the chiral limit on the left, they are expressed in terms of the physical states by

$$\pi_8^0 = \pi^0 - \epsilon\eta - \epsilon'\eta'$$

$$\eta_8 = \cos\theta\ (\eta + \epsilon\pi^0) + \sin\theta\ (\eta' + \epsilon'\pi^0)$$

$$\eta_0 = -\sin\theta\ (\eta + \epsilon\pi^0) + \cos\theta\ (\eta' + \epsilon'\pi^0)$$

A recent global analysis [3] has been performed that uses as input the two-photon decay widths of the η and η' and includes next to leading order chiral corrections as well as $1/N_c$ corrections. It gives: $\epsilon \sim 0.8^\circ$, $\epsilon' \sim 0.3^\circ$ and $\theta \sim -12^\circ$ for these mixing angles. The angles ϵ and ϵ' play an important role in the lifetime of the π^0, decreasing it by approximately 4% [3, 4].

When next to leading order chiral corrections and $1/N_c$ corrections are disregarded, the two-photon partial widths of the η and η' mesons are given by:

$$\Gamma(\eta \to \gamma\gamma) = \frac{\alpha_{\rm em}^2}{64\pi^3}\frac{M_\eta^3}{3F_\pi^2}\left[\cos\theta - \sqrt{8}\sin\theta\right]^2 \tag{5}$$

$$\Gamma(\eta' \to \gamma\gamma) = \frac{\alpha_{\rm em}^2}{64\pi^3}\frac{M_{\eta'}^3}{3F_\pi^2}\left[\sin\theta + \sqrt{8}\cos\theta\right]^2\ . \tag{6}$$

With this one can define a mixing independent quantity, $\mathcal{R}$, involving a combination of the π^0, η and η' widths and their masses, that has a specific value when the mentioned next to leading order corrections are disregarded:

$$\mathcal{R} \equiv \left[\frac{\Gamma(\eta \to \gamma\gamma)}{M_\eta^3} + \frac{\Gamma(\eta' \to \gamma\gamma)}{M_{\eta'}^3}\right] \frac{M_\pi^3}{\Gamma(\pi^0 \to \gamma\gamma)} = 3 \ , \tag{7}$$

The deviation from this relation can be determined by a more precise measurement of the η and η' partial widths, and is a measure of the size of the next to leading order corrections in both the chiral and $1/N_c$ expansions. Such deviations could be determined with an 11 GeV beam at Jefferson Lab. Reference [12] quotes its current value to be $\mathcal{R}_{exp} = 2.5 \pm 0.5(\text{stat}) \pm 0.5(\text{syst})$. A more precise determination of the $\eta, \eta' \to \gamma\gamma$ partial widths will help improve the determination of this observable. For instance, a measurement of the $\eta \to \gamma\gamma$ width to 4%, and of the η' width to 6%, would imply an error in $\mathcal{R}$ of 0.05. This should be enough to pin down a deviation from the leading order value.

The analysis beyond leading order was carried out until recently following the framework of reference [23]. This framework is not fully consistent as it leaves some next to leading order corrections out, in particular those mentioned later involving mixing effects in the coupling constants and next to leading order unnatural parity counterterms. It gives for the decay widths:

$$\Gamma(\eta \to \gamma\gamma) = \frac{\alpha_{\rm em}^2}{64\pi^3} \frac{M_\eta^3}{3F_\pi^2} \left[\frac{F_\pi}{F_{\eta_8}} \cos\theta - \sqrt{8}\frac{F_\pi}{F_{\eta_0}} \sin\theta\right]^2 \tag{8}$$

$$\Gamma(\eta' \to \gamma\gamma) = \frac{\alpha_{\rm em}^2}{64\pi^3} \frac{M_{\eta'}^3}{3F_\pi^2} \left[\frac{F_\pi}{F_{\eta_8}} \sin\theta + \sqrt{8}\frac{F_\pi}{F_{\eta_0}} \cos\theta\right]^2 \ , \tag{9}$$

where F_{η_8} is given from next to leading order Chiral Perturbation Theory excluding the presence of the η' [24]. Most conclusions about the mixing angle θ have been extracted in the past using this approximate framework. The decay constant F_{η_0} and the mixing angle are obtained by fitting to the two-photon decay widths. It should be noted at this point that a more precise measurement of the widths at the level proposed here, will be sensitive to next to leading order corrections, and for this reason these should be implemented within a consistent framework.

In recent times, a framework that implements the chiral and $1/N_c$ corrections was developed [5, 8, 3]. This framework is a faithful representation of low energy QCD, relying only on the validity of the chiral expansion in the strange quark mass and the expansion in $1/N_c$. In particular, this implies the assumption that the η' can still be considered as an approximate Goldstone Boson. The framework predicts that the two-photon decays involve two mixing angles (two-mixing angle scenario [9]). The decay constants of the η and η' associated with matrix elements of the two axial currents $j_{A\mu}^8$ and $j_{A\mu}$ are given by:

$$F_\eta^8 = \cos\theta_8 \ F_8$$

$$F_\eta^8 = \sin\theta_8 \ F_8$$

$$F_\eta^0 = -\sin\theta_0\ F_0$$
$$F_\eta^0 = \cos\theta_0\ F_0. \tag{10}$$

There is also a new low energy constant t_1 to be taken into account at next to leading order in the chiral expansion. It can be estimated using QCD sum rules ($t_1 = -F_\pi^2/m_\rho^4$). With this, the decay amplitudes into two photons defined in equation (4) become:

$$A_{\eta\gamma\gamma} = \alpha(\frac{1}{24\pi F_0 F_8}\sec(\theta_0-\theta_8)(\sqrt{3}F_0\cos\theta_0 - 2\sqrt{6}F_8\sin\theta_8)$$
$$-\frac{\pi}{18\sqrt{3}F_\pi}t_1((4M_K^2-7M_\pi^2)\cos\theta + 2\sqrt{2}(M_K^2+2M_\pi^2)\sin\theta))$$
$$A_{\eta'\gamma\gamma} = \alpha(\frac{1}{8\sqrt{3}\pi F_0 F_8}\sec(\theta_0-\theta_8)(2\sqrt{2}F_8\cos\theta_8 + F_0\sin\theta_0)$$
$$+\frac{\pi}{18\sqrt{3}F_\pi}t_1(2\sqrt{2}(M_K^2+2M_\pi^2)\cos\theta + (-4M_K^2+7M_\pi^2)\sin\theta)) \tag{11}$$

Here θ is the state mixing angle defined earlier.

The fact that there is a well defined theoretical framework makes the η and η' very important states to be studied with precision as a means to further understand fundamental aspects of QCD. In particular, more precise measurements of $\Gamma(\eta\to\gamma\gamma)$ and $\Gamma(\eta'\to\gamma\gamma)$ are crucial to the understanding of the mixing of the two mesons and their decay constants. Indeed, given the shortage of other observables that could be measured with a precision close to that of the two-photon partial widths, these are natural inputs that should be known with good precision. It should be emphasized that more precise inputs at this level will imply a corresponding improvement in the determination of other important observables such as the decays $\eta\to\pi\pi\pi$.

Measurements of the η width have been carried out using the Primakoff effect [13] and $\gamma-\gamma$ fusion in e^+-e^- colliders [16]. These determinations are in clear disagreement. The η' width, on the other hand, has only been measured in e^+-e^- colliders [16]. The current results for the widths, as listed in the Particle Data Book are:

$$\Gamma(\eta\to\gamma\gamma)_{\text{Primakoff}} = 324\pm 46\ \text{eV}$$
$$\Gamma(\eta\to\gamma\gamma)_{\text{Collider}} = 511\pm 26\ \text{eV}$$
$$\Gamma(\eta'\to\gamma\gamma)_{\text{Collider}} = 4.27\pm 0.19\ \text{KeV}$$

Using these inputs, a recent analysis [3] determines $\theta = -12^\circ$, $\theta_8\sim -20^\circ$, $\theta_0\sim\pm 3^\circ$, $F_8\sim 122$ MeV, and $F_0\sim 116$ MeV. These have, however, rather generous errors. A new high quality Primakoff measurement of the η decay and a first Primakoff measurement of the η' can lead to a much more precise determination of these quantities.

One important question to ask is: What would the impact of a more precise measurement of the two-photon partial widths be? Right away, it would imply a corresponding improvement in the determination of the rest of the partial widths, as these are determined using the two-photon widths and the corresponding branching fractions. This would therefore have a

wide ranging impact. One decay that is particularly important is the decay $\eta \to \pi\pi\pi$ (two different final states), which is driven by isospin breaking, and thus gives access to the quark mass ratio $(m_u - m_d)/m_s$. Over time, the theoretical analysis of this decay has progressed to the point that now rather definite predictions can be made [10]. However, substantial discrepancy remains with the corresponding partial widths determined in the fashion just mentioned, with the theoretical width being smaller than the experimental one. One important issue to be clarified here is whether the quoted experimental width $\Gamma(\eta \to \gamma\gamma)$ is too large, or whether the convergence of the chiral expansion is not as good as expected. A more precise measurement would thus clarify this important issue. Note that the decays $\eta \to \pi\pi\pi$ play a crucial role in determining the quark mass ratio m_u/m_d. In a very elegant analysis, Leutwyler [11] constructed a relation, now called Leutwyler's ellipse, given by:

$$\left(\frac{m_u}{m_d}\right)^2 + \frac{1}{\mathcal{Q}^2}\left(\frac{m_s}{m_d}\right)^2 = 1 \tag{12}$$

where the semi-major axis Q is given by the ratio:

$$\mathcal{Q}^2 = \frac{m_s^2 - \hat{m}^2}{m_d^2 - m_u^2} \tag{13}$$

with $\hat{m} = (m_u + m_d)/2$.

One way to determine $\mathcal{Q}$ is given by a ratio of meson masses:

$$\mathcal{Q}^2 = \frac{M_K^2}{M_\pi^2}\frac{M_K^2 - M_\pi^2}{(M_{K^0}^2 - M_{K^+}^2)_{QCD}}[1 + O(m_{quark}^2)] \tag{14}$$

The chief problem in extracting $\mathcal{Q}$ from this relation arises from the uncertainties in the electromagnetic contributions to the $K^0 - K^+$ mass difference. Another way to extract $\mathcal{Q}$ is by means of $\eta \to \pi\pi\pi$ decays that have negligibly small electromagnetic corrections due to chiral symmetry. The second approach thus represents a more sensitive probe of the symmetry breaking generated by $m_d - m_u$, and has the potential to deliver accurate quark mass ratios [6]. As emphasized by Leutwyler [11], the main errors in determining $\mathcal{Q}$ using $\eta \to \pi\pi\pi$ decays is due to the experimental uncertainties in the partial width $\Gamma_{\eta\to\pi\pi\pi}$ that are determined by the two-photon widths $\Gamma_{\eta\to\gamma\gamma}$ and branching ratio. The two different methods of measuring $\Gamma_{\eta\to\gamma\gamma}$ (photon-photon collisions and Primakoff effect) yield conflicting results, as shown in figure 1. This is one important example of the impact that the more precise measurement of the η and η' two-photon widths would have for determining fundamental parameters of QCD. On the side of the η', perhaps one of the most interesting questions has to do with the nature of the η': is it after all an approximate Goldstone Boson or not? The more precise measurements together with the theoretical framework we have in place would help answer that question via a global analysis of the different processes involving the η and η'. For instance, if such an analysis shows that the size of the $1/N_c$ corrections is natural, this would imply that it is consistent to think about the η' as an approximate Goldstone Boson. In summary, it is clear that a more precise experimental knowledge of the two-photon partial widths will have an important impact in our understanding of fundamental issues in QCD.

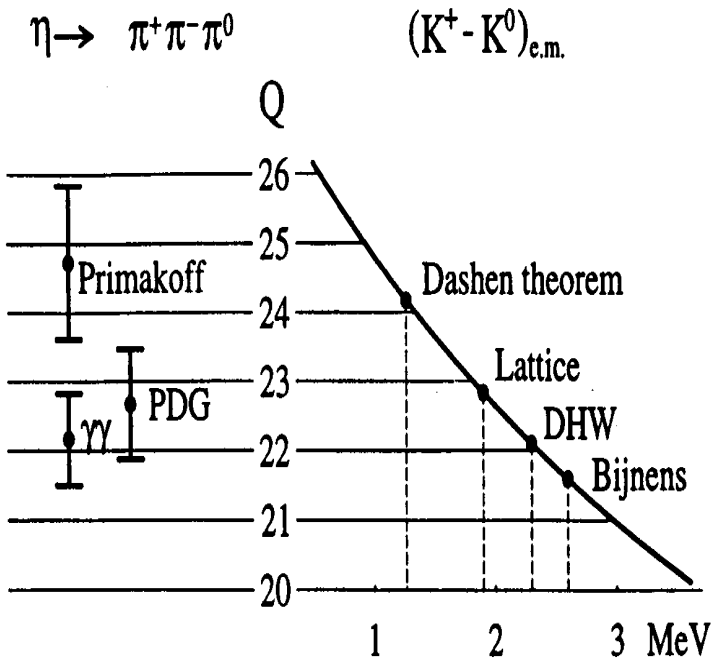

Figure 1: The importance of $\Gamma_{\eta\to\gamma\gamma}$ in the measurement of $\mathcal{Q}$. The l.h.s. indicates the values of $\mathcal{Q}$ corresponding to the Primakoff and collider experimental results for the $\Gamma_{\eta\to\gamma\gamma}$. The r.h.s. shows the results for $\mathcal{Q}$ obtained with four different theoretical estimates for the electromagnetic self energies of the kaons. Taken from Ref. [11].

Using Primakoff electroproduction it is also possible to measure the transition form factors $F_{\gamma\gamma^* P}$ for one off shell photon. So far, the transition form factors have been determined in collider experiments [17] with relatively large Q^2 ($Q^2 \geq 0.6$ GeV^2), except for the recent measurement for the η' measured by the L3 collaboration [18] where Q^2 is as low as 0.05 GeV^2 but with big error on Q^2. Measurements of the π^0, η and η' transition form factors at very low Q^2 (~ 0.001–$0.5 GeV^2$) are particularly important in the extraction of the slope of the transition form factor, and to measure the size of the meson's electromagnetic interaction radius model independently. Currently, there is no first principles theoretical determination of the form factors. In ChPT there are two sources of contributions [14], one is the long distance contribution from meson loops, and the other is a counterterm or short distance contribution. ChPT pins down the first, and for the second a model is needed. The long distance contributions are small, as they only provide a small fraction of the fall off of the form factor. The simplest model is to neglect the long distance contributions and assume a monopole type form factor,

$$F(Q^2) = \frac{\Lambda^2}{Q^2 + \Lambda^2}.$$

Using such a model, the available data at high Q^2 fit very well with a scale $\Lambda \sim 0.75 - 0.85$ GeV. The vector meson dominance (VMD) model is therefore an excellent model to fit the current data ($Q^2 > 0.6 GeV^2$).

A determination of the slope of the π^0 and η form factors would allow one to uniquely fix a low energy constant $\mathcal{O}(p^6)$ in the effective chiral Lagrangian[14] [4]. With a measurement of the η' form factor slope, one could also have a clear test of how good the U(3) flavor symmetry implied by the large N_c limit holds. In this limit the same low energy term of order six should determine all slopes. In addition, one important reason to better understand the transition from factors of π^0, η and η' is that pseudoscalar exchange is the major contribution to the hadronic light-by-light scattering part of the muon anomalous magnetic moment[7] and is thus clearly crucial for future measurements of a_μ that search for "new physics" beyond the Standard model. A summary of the present situation is given in Appendix I.

In summary, the appearance of the chiral anomaly and the prediction of the Goldstone Bosons due to the spontaneous breaking of chiral symmetry are two basic characteristics of QCD at low energies. Understanding the properties of pseudoscalar mesons which involve both Goldstone Bosons and the chiral anomaly are fundamentally important in confinement scale QCD. The three neutral pseudoscalar mesons π^0, η and η', with the first two being Goldstone Bosons as their masses would vanish in the chiral limit, while the η' is not due to the chiral anomaly, represent one of the most interesting and important systems in low energy QCD. This system contains fundamental information about the effects of SU(3) and isospin breaking by the u, d, and s quark masses, leading to important mixing effects among the mesons, as well as about two types of chiral anomalies. A study of the two-photon decays of the π^0, η and η' and their transition form factors at very small Q^2 will allow one to determine the η, η' mixing angle, the pattern of decay constants according to the two-mixing-angle scenario, and one low energy constant $\mathcal{O}(p^6)$ in the chiral Lagrangian that determines the slope of the form factors. It will provide a test of the low energy limit of QCD in a relatively clean setting, and help us better understand the origin and dynamics of chiral symmetry breaking. In addition, a high quality measurement of the η two-gamma decay width will provide a clear answer to the fundamental question of the $m_d - m_u$ quark mass difference by improving the precision of the $\eta \to \pi\pi\pi$ width. The study of the η' will lead to a better understanding of the η' mass puzzle and in general about its nature. As the lifetimes of the η and η' listed in the Particle Data Book were determined by the two-photon decay widths of those particles, these proposed measurements will give a better understanding of the properties of the η and η' in general.

4 Radiative Widths of Pseudoscalar Mesons

In the summer of 2002, the JLab PAC22 reviewed an approved experiment of the PrimEx Collaboration (E99-014, currently E02-103) to perform a precision measurement of the π^o lifetime in Hall B using photoproduction in the Coulomb field of a nucleus, and assigned to it an A rating. The proposed measurement at the $\simeq$1.4% accuracy level fills an important gap between theoretical and experimental knowledge of the π^o lifetime. New possibilities to measure the analogous decay widths for the η and η', however, will open up with the

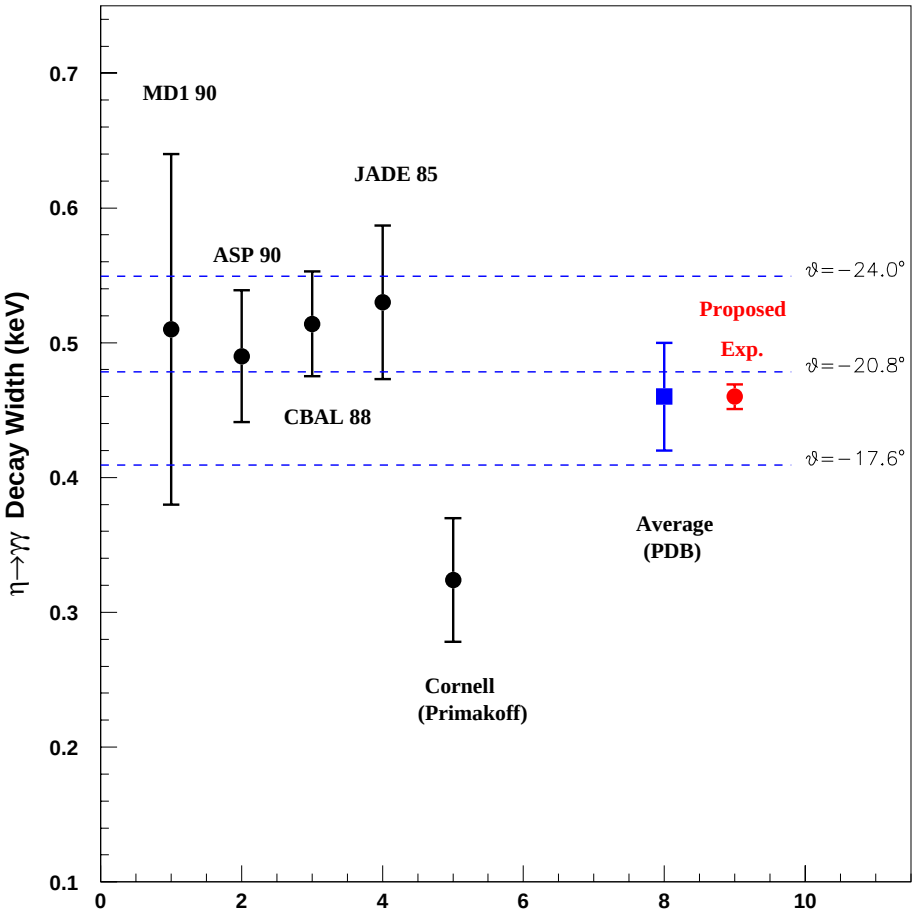

Figure 2: Two-photon decay width for the η meson. Points 1 through 4, are the results of e^+e^- collisions (for references, see[16]), point 5 is the result of a Primakoff experiment[13]. Point 6 is the Particle Data Book[16] average based on the first five points. Point 7 is the expected error for our future experiment, arbitrarily plotted to agree with the Particle Data Book average value. The plotted uncertainties combine the statistical and systematic errors in quadrature (see table 1). The three lines are the widths for different η-η' mixing angles as indicated. See reference[15].

availability of 11 GeV beams. These are described below.

4.1 Previous Measurements of the η and η' Radiative Widths

The present experimental knowledge of the η meson width is presented in figure 2[16], along with the projected measurement which could be made with 11 GeV at Jefferson Lab. Most of the measurements in the figure have been performed using two photon interactions in e^+e^- collisions. One exception is the Cornell measurement of the η width[13] via the Primakoff effect. This gives a width which is significantly lower (at the 3σ level) than those from e^+e^- collisions. Using the same apparatus, the Cornell group measured the $\Gamma(\pi^0 \to \gamma\gamma) = 7.93 \pm 0.39$ eV, in good agreement with the world average value of 7.74 ± 0.55 eV. As such, the η width should be remeasured by the Primakoff process using state-of-the-art experimental techniques to resolve this discrepancy.

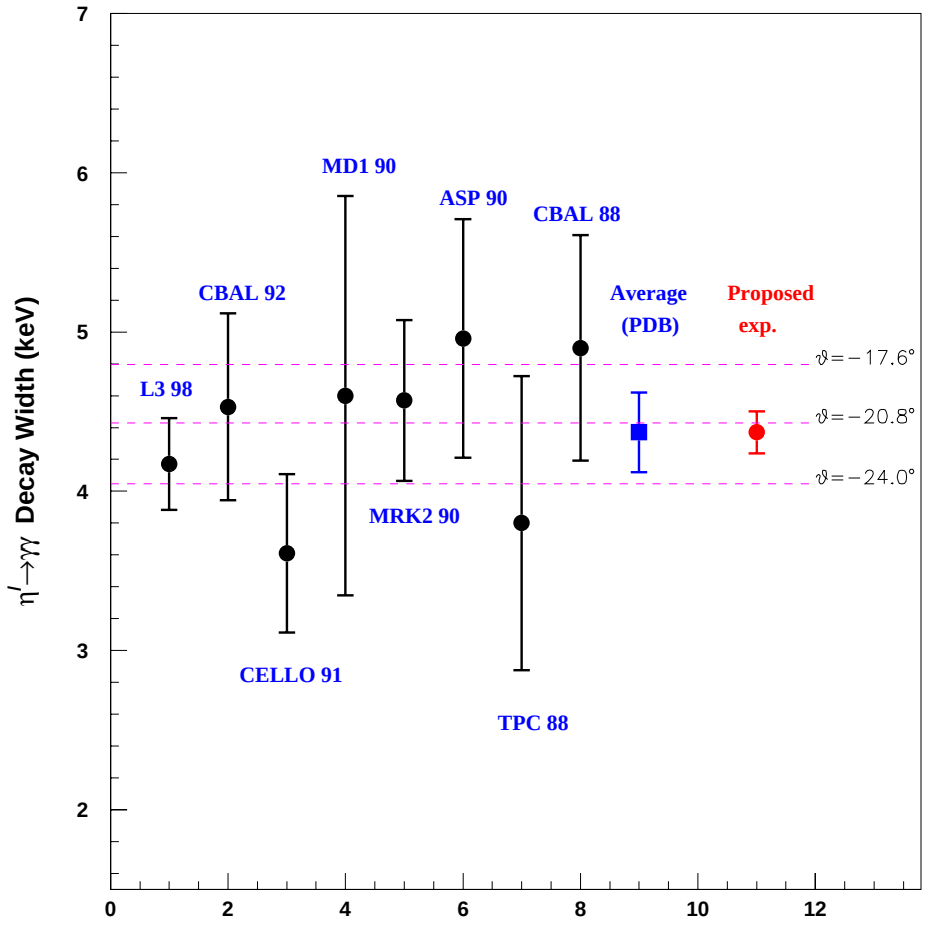

Figure 3: Two photon decay width for the η' meson. First 8 points are the results of e^+e^- collision experiments (for references see[16]). Point 9 is the Particle Data Book average based on the points 2–8. The last point is expected error of the proposed future experiment (5%). The plotted uncertainties combine the statistical and systematic errors in quadrature. The three lines are the widths for different $\eta - \eta'$ mixing angles as indicated.

The present status of the η' meson width is presented in figure 3[16], with the last point being the projected measurement at Jefferson Lab. All previous measurements use the $e^+e^- \to e^+e^-\gamma^*\gamma^* \to e^+e^-\eta'$ process, and the formation of the η' is identified by measuring its decay particles.

The horizontal lines in figure 2 and figure 3 show the sensitivity of the η and η' two photon decay widths to the $\eta - \eta'$ mixing angle. Venugoapl and Holstein[15] have determined the $\eta - \eta'$ mixing angle by simultaneously fitting data from η,η' reactions involving the anomaly $(\eta, \eta' \to \gamma\gamma, \pi^+\pi^-\gamma)$. Their result, $\theta = -20.8^o \pm 3.2^o$, is shown in the figures. It can be seen that the mixing angle is strongly dependent on the widths of η and η'. An improved measurement will provide an important constraint on this parameter. In addition, the figures also indicate that the η and η' two photon decay widths have opposite correspondence to the mixing angle. This would allow one to cross check the experimental systems if one measures

both the η and η' two-gamma decay widths.

4.2 Measurement of the η and η' Radiative Widths via the Primakoff Effect

We propose to use a tagged photon beam obtained from the 11 GeV electrons to measure the widths of the $\eta, \eta' \to \gamma\gamma$ decays via the Primakoff effect. The Primakoff effect is shown in figure 4. Mesons are produced by the interaction of a real photon with a virtual photon from the Coulomb field of the nucleus. The formation of mesons will be identified through the invariant mass of two decay photons from the $\eta/\eta' \to \gamma\gamma$ reaction, and the meson production angles will be reconstructed by detecting the η/η' decay photons as well.

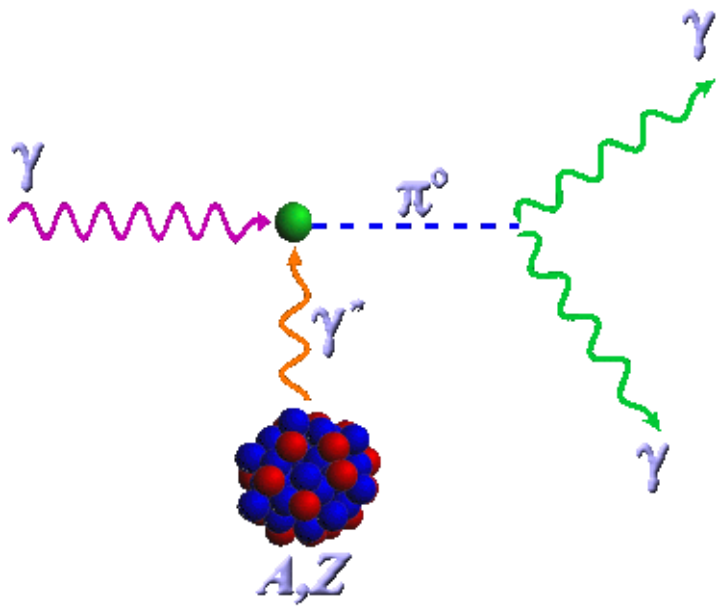

Figure 4: Schematic representation of the Coulomb photoproduction of neutral mesons (Primakoff effect).

The production of mesons in the Coulomb field of a nucleus by real photons is essentially the inverse of the decay $\eta, \eta' \to \gamma\gamma$, and the cross section for this process thus provides a measure of the η, η' two-photon decay widths.

For unpolarized photons, the Primakoff cross section is given by[27]:

$$\frac{d\sigma_P}{d\Omega} = \Gamma_{\gamma\gamma} \frac{8\alpha Z^2}{m^3} \frac{\beta^3 E^4}{Q^4} |F_{e.m.}(Q)|^2 sin^2\theta_m \tag{15}$$

where $\Gamma_{\gamma\gamma}$ is the decay width of the η or η', Z is the atomic number, m, β, θ_m are the mass, velocity and production angle of the mesons, E is the energy of the incoming photon, Q is the momentum transferred to the nucleus, and $F_{e.m.}(Q)$ is the nuclear electromagnetic form factor, corrected for final state interactions of the outgoing η or η'.

The Primakoff effect is not the only mechanism for meson photoproduction at high energies. There is coherent background from strong production of η,η' in the nuclear hadronic field, and an interference between the strong and Primakoff production amplitudes. The full cross section is given by:

$$\frac{d\sigma}{d\Omega_\pi} = \frac{d\sigma_P}{d\Omega} + \frac{d\sigma_C}{d\Omega} + \frac{d\sigma_I}{d\Omega} + 2 \cdot \sqrt{\frac{d\sigma_P}{d\Omega} \cdot \frac{d\sigma_C}{d\Omega}} cos(\phi_1 + \phi_2) \tag{16}$$

where the Primakoff cross section, $\frac{d\sigma_P}{d\Omega}$, is given by equation (9). The nuclear coherent cross section is given by:

$$\frac{d\sigma_C}{d\Omega} = C \cdot A^2 |F_N(Q)|^2 sin^2\theta_m \tag{17}$$

and the incoherent cross section is:

$$\frac{d\sigma_I}{d\Omega} = \xi A(1 - G(Q)) \frac{d\sigma_H}{d\Omega} \tag{18}$$

where A is the nucleon number, $Csin^2\theta_m$ is the square of the isospin and spin independent part of the neutral meson photoproduction amplitude on a single nucleon, $|F_N(Q)|$ is the form factor for the nuclear matter distribution in the nucleus (corrected for final state interactions of the outgoing mesons), ξ is the absorption factor of the incoherently produced mesons, $1 - G(Q)$ is a factor which reduces the cross section at small momentum transfer due to the Pauli exclusion principle, and $\frac{d\sigma_H}{d\Omega}$ is the η,η' photoproduction cross section on a single nucleon. The relative phase between the Primakoff and nuclear coherent amplitudes without final state interactions is given by ϕ_1 and the phase shift of the outgoing meson due to final state interactions in the final state is given by ϕ_2.

The classical method of extracting the Primakoff amplitude from the measured differential cross sections in the forward direction relies on the different characteristic behaviors of the production mechanisms with respect to the production angle. The Primakoff cross section is zero for mesons emitted along the incident photon direction, has a sharp maximum at a very small angle, and falls at larger angles as shown in figure 5 for the ^4He nucleus. It is proportional to Z^2, and its peak value is roughly proportional to E^4. The nuclear coherent cross section for spin zero nuclei is also zero in the forward direction, but has a broad maximum outside the angular region of the Primakoff effect, and falls at larger angles as shown in figure 5, where the amplitudes are normalized to the Cornell data[13]. However, as can be seen from figure 5, there are still two types of contributions under the Primakoff peak–the extended tail of the nuclear coherent mechanism, and the interference term between the two amplitudes as described above. The interference term amounts to a relatively large contribution and is also more difficult to identify since in addition to the knowledge of both amplitudes, it also requires knowing the relative phase angle between them. Therefore, a precision determination of the contribution from the background amplitudes under the

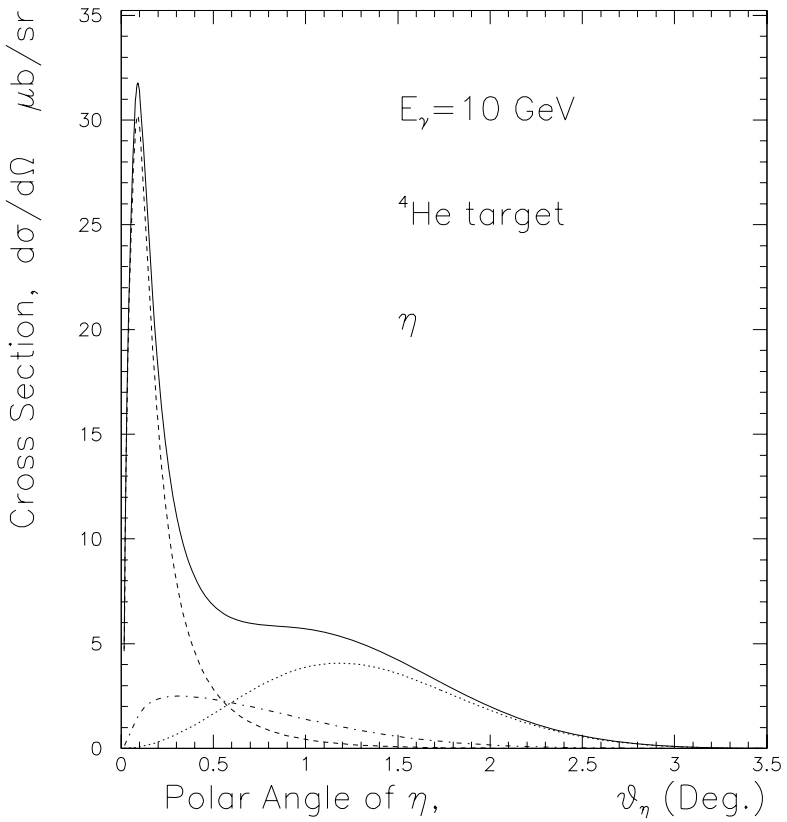

Figure 5: Differential cross sections (electromagnetic and nuclear) for the $\gamma + {}^4He \to \eta + {}^4He$ reaction at small angles at 10 GeV. The solid line is the total differential cross section from all the process, the dashed line is from Primakoff process, the dotted line is from the nuclear coherent process, and the dot-dash line is from the interference of the Primakoff and nuclear coherent processes.

Primakoff peak requires good experimental information on the nuclear amplitude outside of the Primakoff region. This can be experimentally achieved by using very light spin zero nuclei as production targets. Since form factors for light nuclei fall slowly with momentum transfer, such targets are well suited for measuring the nuclear part at large angles, thereby determining the contribution under the Primakoff peak.

In this proposal we are suggesting a simultaneous measurement of the differential cross sections at the forward angles on two targets: the proton and ^4He. ^4He has several advantages over other targets. First, it is a very compact nucleus (with a nucleon threshold of $\sim$20 MeV), which will greatly enhance coherence production. Second, its form factor is very well known and falls slowly with momentum transfer. In addition, it is a spin zero nucleus, which will largely suppress the spin flip amplitude contribution close to zero degrees. The nuclear coherent amplitude in principle can be expressed in terms of the single-nucleon

photoproduction amplitudes, properties of the nuclear ground state, and the interaction of mesons in nuclei[30].

The use of hydrogen and helium targets will greatly help to solve the difficulties of the Cornell $\eta \to \gamma\gamma$ experiment to extract the coherent contribution under the Primakoff peak as pointed out in the Particle Data Book.[31] As a production target, hydrogen is especially promising because it makes possible the selection of exclusive π^o p events through a missing mass cut. In principle this can be done with the many-body nuclear targets, but in practice there is the complication due to inelastic transitions and breakup channels at low excitation energy. For the nuclear targets, dynamical considerations (*i.e.* momentum transfer and the nuclear form factors) are usually invoked to ensure that coherency is satisfied to a high degree, whereas for the proton target it will be possible to guarantee coherency through kinematic cuts. The missing mass resolution that can be expected in a 12 GeV experiment, and how that resolution can be optimized, are presently under study.

The cross section calculations that are needed for a proton target are in progress. For the Primakoff amplitude it is important to consider both charge and magnetic scattering from the target. (For a spin zero nucleus there is no magnetic contribution.) For the coherent background amplitude, which is expected to be dominated by ρ and ω exchanges, calculations based on the Regge model developed by Vanderhaeghen, Guidal, and Laget [32] will be performed. This formalism has been successfully used in extractions of the pion electromagnetic form factor from pion electroproduction data. Finally, it should be noted that a proof-of-principle exists for doing a Primakoff experiment on the proton. In the early 1970's a group at DESY measured forward π^o photoproduction on the proton [33]. Their data clearly exhibit a Primakoff peak at forward angles, and the pion lifetime obtained from the data agrees, within quoted errors, with the accepted value.

The cross section for the Primakoff effect to produce an η on ^4He is presented in figure 5. Compared to the Primakoff effect to produce a π^0, η production has a significantly smaller cross section and peaks at relatively larger production angles. This is a consequence of the much larger mass of the η which increases the momentum transfer at a given production angle. As a result, the Primakoff peak is harder to distinguish from the nuclear coherent peak. There are two ways to ameliorate this problem. One is to go to higher photon energies, which, in addition to increasing the Primakoff cross section ($\sigma_P \propto E^4$), will push the Primakoff peak to smaller angles ($\theta_{Primakoff} \sim \frac{m^2}{2E^2}$) as compared to those of the nuclear coherent effect ($\theta_{NC} \sim \frac{2}{EA^{\frac{1}{3}}}$). As such, the proposed 12 GeV upgrade to the CEBAF accelerator is vital to these measurements. Another improvement is to use lighter targets such as ^1H, ^4He or ^{12}C, which are more bound compared to heavier nuclei, thereby enhancing coherency. In addition, due to the A dependence just mentioned, one would expect the nuclear coherent mechanism to peak at larger angles for lighter nuclei. We argue that by simultaneously going to higher photon energies and using lighter Primakoff production targets, one can make clean measurements of the widths.

4.3 Experimental Setup for η/η' Width Measurement

We propose to use a tagged photon beam to produce the η/η' mesons, and to detect multiphoton final states in a calorimeter. In addition to the 11 GeV upgrade to the CEBAF accelerator, such measurements would require (1), a high energy photon tagging system, and (2), a $1.5m \times 1.5m$ multichannel calorimeter consisting of high resolution lead tungstate scintillating crystals to detect decay photons from the meson decay. Details of this instrumentation are given below.

4.3.1 High Energy Photon Tagging System

This proposed program requires a high intensity, high precision 11 GeV photon tagging system. The existing Hall B tagger is designed for a maximum of 6 GeV and at present, there are no known plans to bring it to the capability to tag higher energy photons. A high energy photon tagging system has been proposed by the Hall D collaboration[25], the design of which is optimized to provide linearly polarized photon beams with high collimation of the bremsstrahlung photons. This requires a relatively long distance ($\sim$90 m) for photons from the bremsstrahlung radiator to the collimators and makes this part of the photon beam line inaccessible. The experimental program proposed here simultaneously requires high precision in both photon flux control (at the 1% level) and angular resolution for forward meson production ($\sim$0.3 mrad). The angular resolution requires the photon beam spot at the Primakoff production target to be minimized ($\sim$1 mm). The optimal configuration for these measurements is thus one in which the physics target is relatively close to the bremsstrahlung converter and the photon beam is uncollimated. As such, the proposed Hall D tagging system is unable to simultaneously provide these two criteria.

In this proposal, we are suggesting the construction of a photon tagging system based on a new approach involving parallel transport of both the photon and primary electron beams through the beam line up to the beam dump. Two identical 'C-type' dipoles will displace the initial electron beam and make it parallel to the photon beam produced in the bremsstrahlung radiator (10^{-4} r.l. Au) placed just upstream of the first dipole (see figure 7). The parallel displacement depends on two parameters – the integrated field in the dipoles and the distance between them.

We impose the following requirements for the design of this tagging system. First, it should be a functional, relatively low cost system. Second, its size and design should allow flexibility to potentially incorporate it into any of several upgraded Halls currently being contemplated at Jefferson Laboratory.

In the current design (see figures 6 and 7) two standard C-dipoles with a $\int Bdl = 5kGmeter$ placed 2 meters apart will provide a $5cm$ parallel displacement of electron and photon beams. We are planning to use $3cm$ diameter and $10cm$ long liquid Hydrogen (LH2) and Helium-4 (LHe4) targets placed downstream of the second dipole. To minimize beam background, we are planning to use a set of lead shielding walls (20 r.l. thick) surrounding the second dipole and one with a narrow hole ($8cm$ width, $2cm$ in height) in the middle of a wall placed $1m$ downstream of the second dipole and just upstream of the physics targets. The post-bremsstrahlung electrons will be deflected in the first C-Dipole and detected

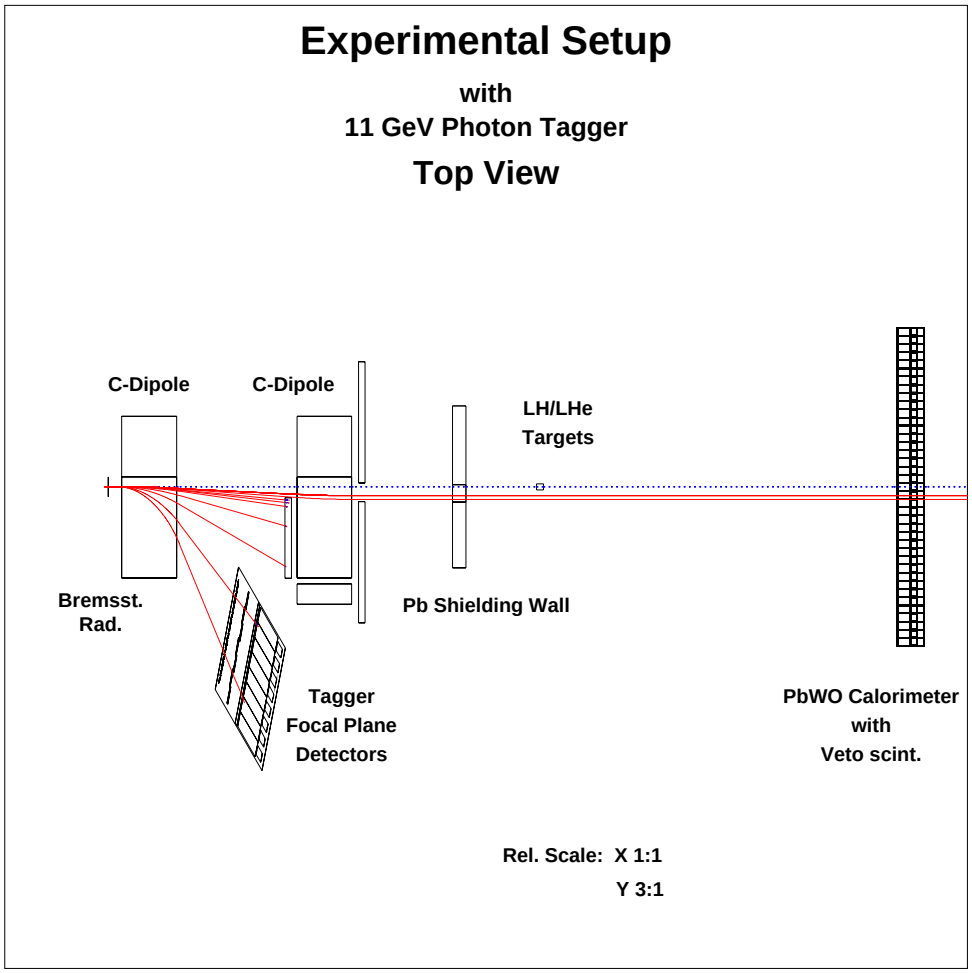

Figure 6: Top view of the experimental setup for η and η' two–gamma decay width measurements. It includes (1) a photon tagging system, and (2) a $1.5m \times 1.5m$ multichannel calorimeter.

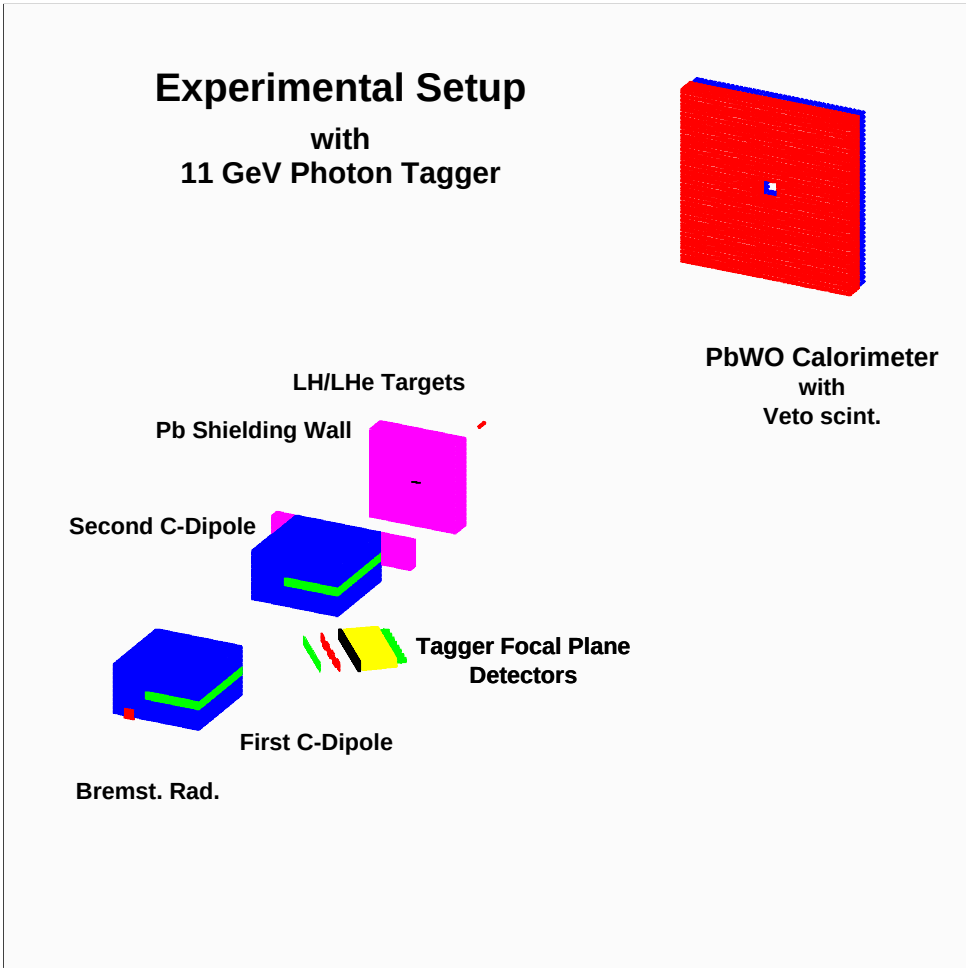

Figure 7: Side view of the experimental setup for η and η' two–gamma decay width measurements. It includes (1) a photon tagging system, and (2) a $1.5m \times 1.5m$ multichannel calorimeter.

by the tagger focal plane detectors (see figure 8). We are planning to use three layers of detectors. The first will be highly segmented scintillating detectors for energy definition of the post-bremsstrahlung electrons. The second plane of seven scintillators will provide fast timing for the tagger; eight lead glass detectors ($8.5 \times 8.5 \times 35 cm^3$) in the third plane will significantly improve background suppression. A $2.5cm$ thick Al absorber plate just in front of the lead glass detectors will cut down the low energy charged particle background produced in the shower counters. In this design, we are focusing on a high energy photon tagger only. A focal plane with a length of $\sim 60cm$ will provide tagged photons of energy $E_\gamma = 10.0 - 10.5 GeV$.

The decay particles from the forward produced neutral mesons will be detected in the high resolution Electromagnetic Calorimeter. For this purpose, we are proposing to upgrade the current HYCAL detector such that it is composed entirely of $PbWO_4$ modules with a total overall size of $1.5 \times 1.5 m^2$. This will consist of a 75×75 matrix of crystals (5625 $PbWO_4$ crystals total), with a central $12 \times 12 cm^2$ hole (6×6 crystals removed) in the middle for the passage of the beams. This calorimeter will be placed at a variable distance $(5 - 10m)$ downstream from the production targets to provide the optimal acceptance for each experiment.

4.3.2 Beam Backgrounds

As is typical of all conventional tagging experiments, the beam backgrounds for the decay width measurements will be dominated by the post bremsstrahlung electrons which lose relatively little energy in the bremsstrahlung radiator and hit the tagger structure. Conventional taggers also have an additional source of background from the electron beam dump. Since in the high energy tagging system proposed here the electron beam will be dumped together with the photon beam far from the tagger, this setup should be largely free of this second type of background. Nevertheless, in the geometry proposed here a significant number of electrons will hit the shielding structure close to the beam line (see figure 6). The forward electromagnetic calorimeter will be centered on the beam line, 5 to 10 m downstream of the production target. Therefore, it will be very sensitive to the tagging setup configuration. There can be two basic approaches to the geometrical design of the calorimeter. One way is to remove a 6×6 matrix of crystal modules from the center of the calorimeter for the beam to pass through. This maximizes and simplifies the geometrical acceptance. The next option is to remove all the modules from several rows of the calorimeter in the dispersive plane of the electron beam (the horizontal plane for this design). Here, we explore the first option for reasons mentioned above.

To estimate the background level and to optimize the experimental setup, we have performed a Monte Carlo simulation based on the GEANT package. The experiment will typically run with an electron current of $75 nAmps$, which will produce 5×10^7 equivalent γ's/sec on the 10^{-4} Au radiator. We have simulated a total of 10^8 electrons through the setup with the following parameters: a 10^{-4} r.l. Au bremsstrahlung radiator; tagging system with a two C-type dipoles and a set of lead shielding walls, as is shown in figure 6; a 10 cm liquid ^4He target in the photon beam; and the electromagnetic calorimeter with a

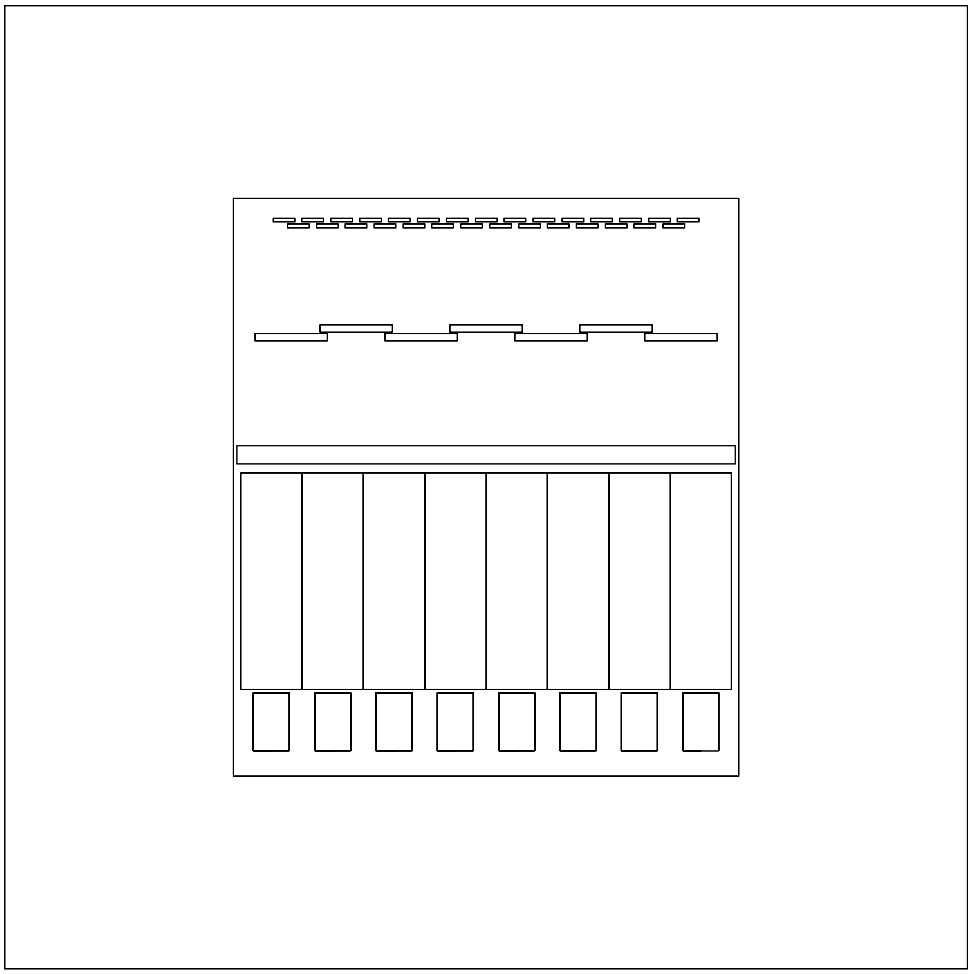

Figure 8: Focal plane detectors for the proposed high energy tagging system including two rows of segmented scintillators (top) and lead glass detectors (bottom).

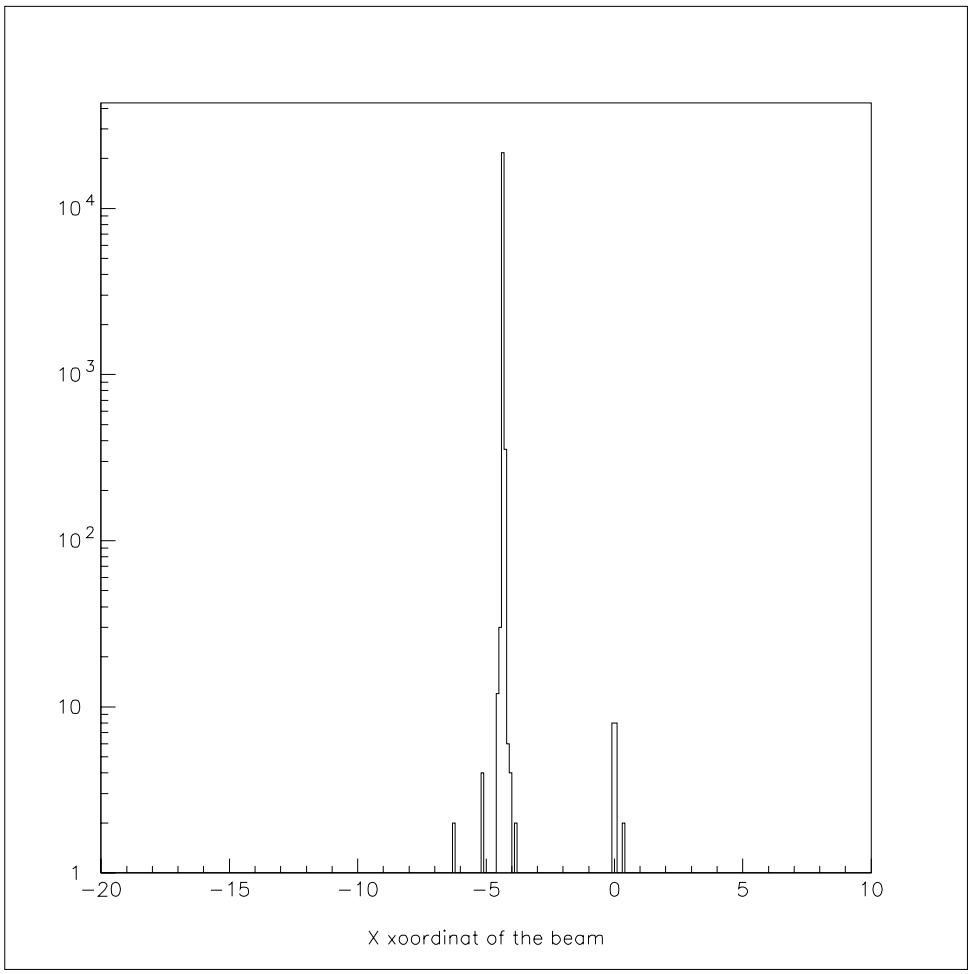

Figure 9: Relative displacement of electron and photon beams in the proposed high energy photon tagging system.

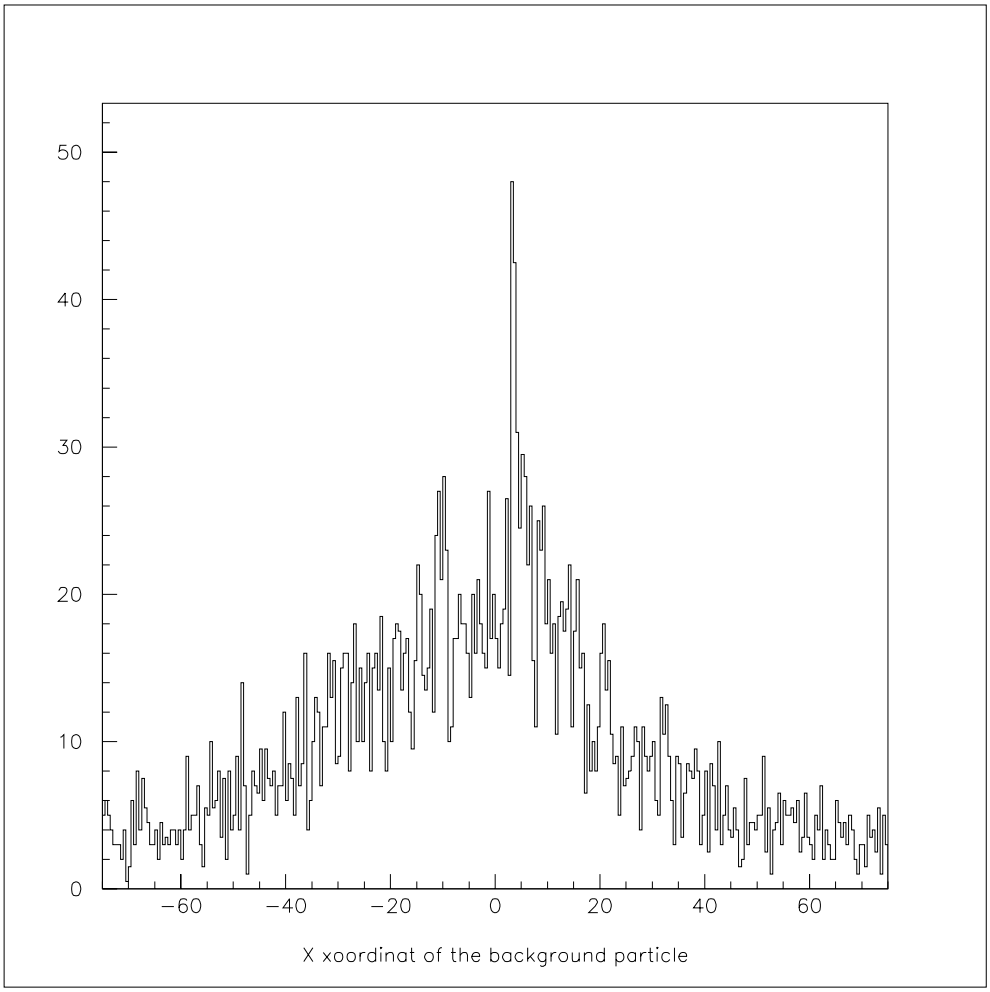

Figure 10: Background events in the calorimeter projected to the horizontal (dispersive) plane for a photon tagging run.

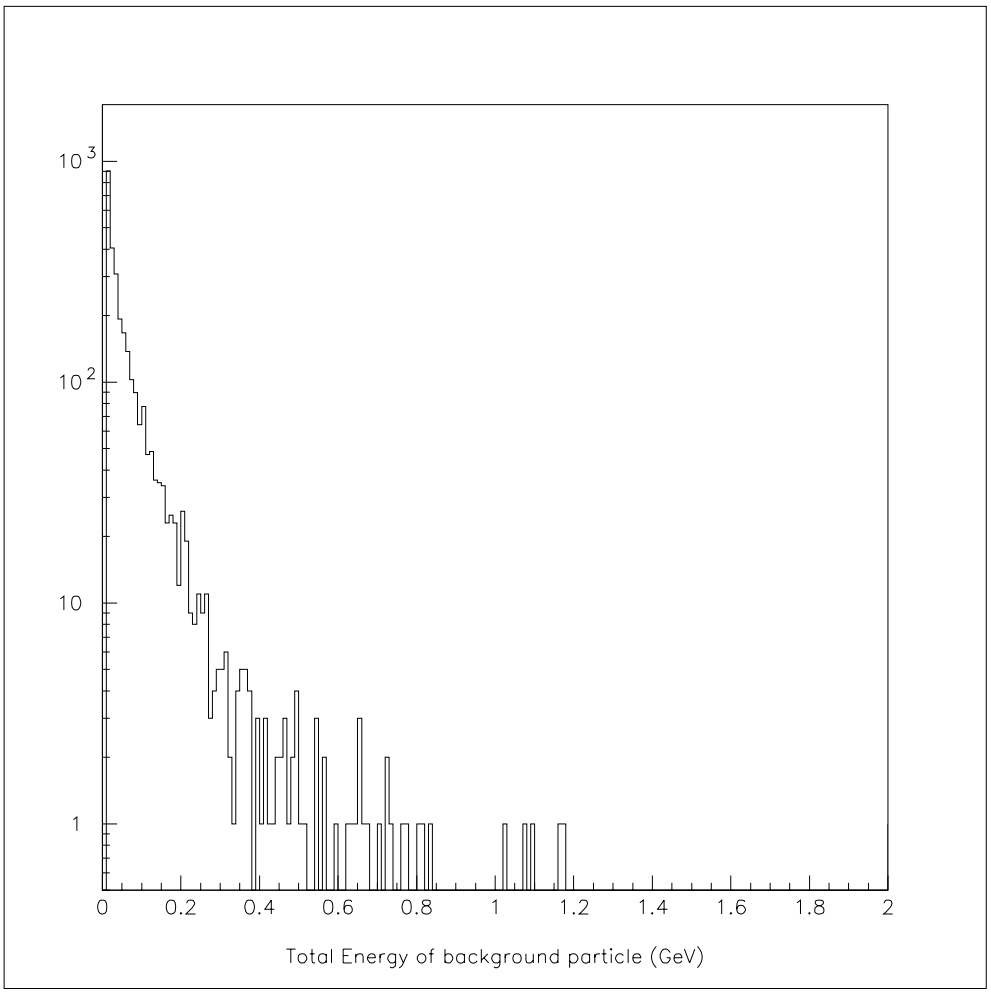

Figure 11: Energy distribution in calorimeter corresponding to the events in figure 10 (photon run).

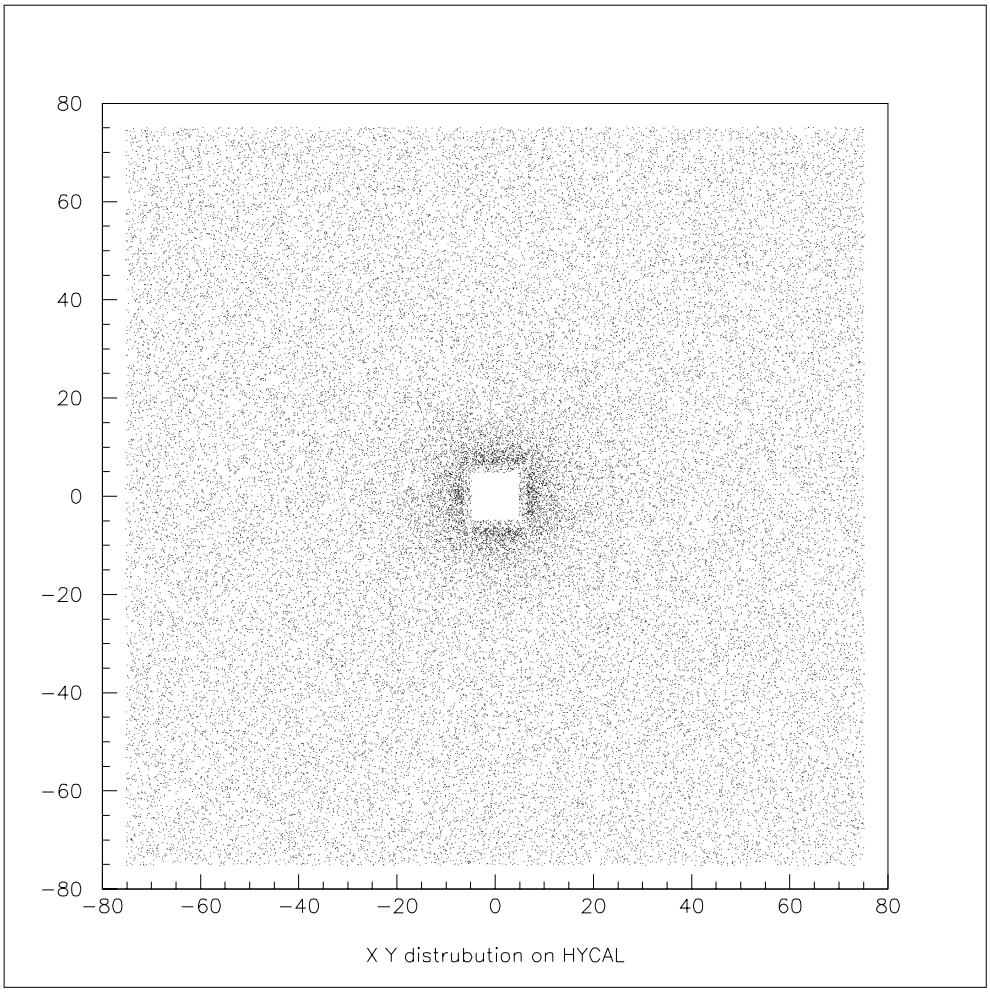

Figure 12: $x - y$ hit distribution of particles on the face of the proposed calorimeter for an electron run.

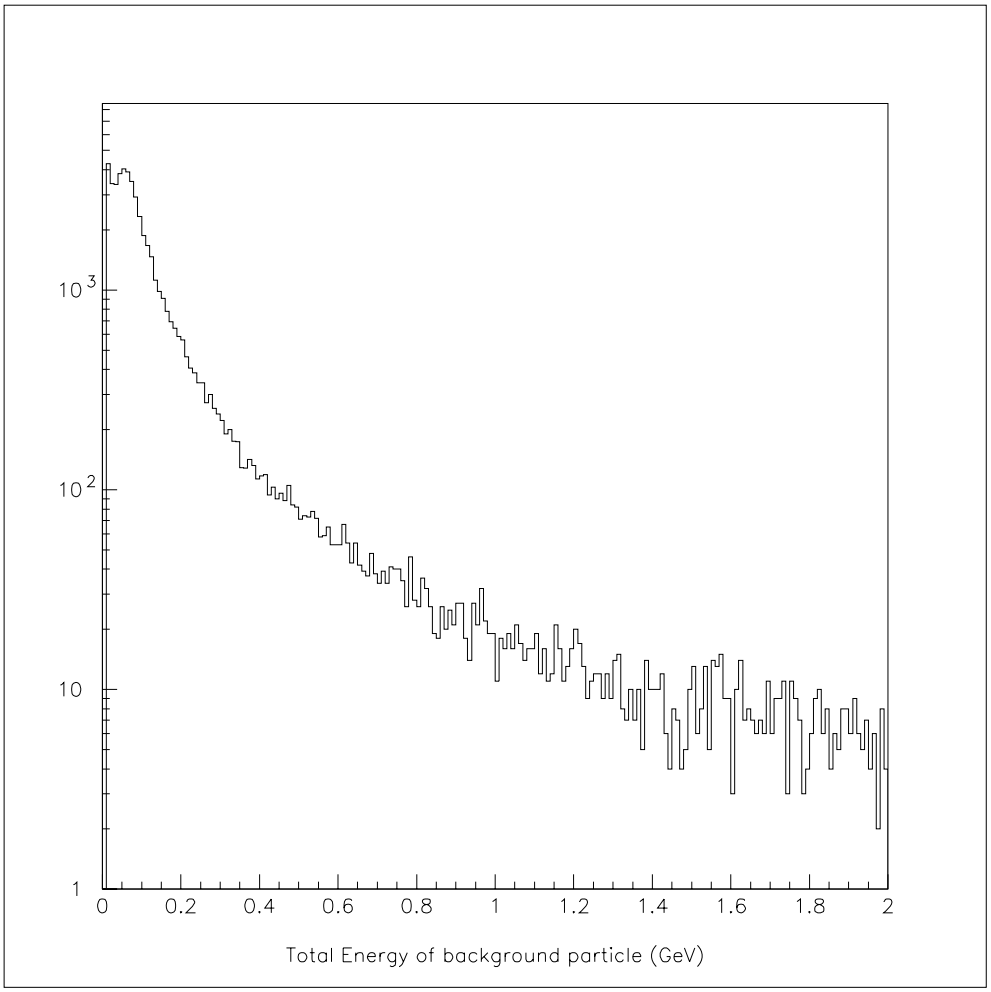

Figure 13: Energy distribution corresponding to the events on the calorimeter in figure 12 from an electron run.

$12 \times 12 cm^2$ central hole. This would be equivalent to ~ 200 microseconds beam time in an experiment. The resulting distribution of background events on the calorimeter is shown in figure 10, projected onto the horizontal axis. The energy distribution of these events is shown in figure 11. Based on these simulations, the electromagnetic calorimeter will have ~ 200 kHz rate with energy bigger than 0.5 GeV. The expected rate per crystal module is 0.4 kHz on average. These numbers are quite promising for the proposed tagging system. Further optimization of the location and thickness of the lead shielding is underway.

A similar experimental setup will be used for the transition form factor measurements to be described below. For those experiments the bremsstrahlung radiator will be removed and there will be no magnetic field in the tagger dipoles. For this configuration we have simulated 2×10^7 electrons through the setup. This is equivalent to 30 microseconds of running with an electron beam current of 100 nAmp. Figure 12 shows the two dimensional distribution of events on the calorimeter. The energy distribution of those events is shown in the figure 13. With a 0.5 GeV threshold, the total rate in the calorimeter is expected to be 80 MHz. The high segmentation of the calorimeter (5625 $PbWO_4$ modules) will bring this rate down to the level of 10 kHz per module.

4.3.3 The Electromagnetic Calorimeter

Photons resulting from η and η' decay and scattered electrons in the transition form factor measurements will be detected in the highly segmented array of a shower calorimeter (ECAL) located downstream of the target. Currently, the PrimEx Collaboration is constructing a hybrid shower calorimeter for the π^0 life time experiment in Hall B, as shown in figure 14. This will be ready for commissioning in Fall of 2003. We propose to use a somewhat larger version of this detector for these experiments. It will be about 150×150 cm^2 in the dimensions transverse to the beam. The calorimeter is designed to measure both the position and the energy of electromagnetic showers using a two dimensional matrix of radiators ($PbWO_4$ crystals). This will be accomplished by choosing the cross section of the individual counters small enough so that the energy leakage into adjacent counters can be used to determine the position of the shower axis.

The Primakoff cross section peaks at extremely small angles ($\theta_\eta = 0.1^o$ at $E_\gamma = 10 GeV$) and therefore the experimental setup must have sufficient resolution for the η production angle in order to identify and extract the Primakoff amplitude. This resolution depends strongly on the decay photon energy and position resolutions of the calorimeter. As such, this detector will be constructed from lead tungstate ($PbWO_4$) crystals of size $2 \times 2 \times 18 cm^3$. In our beam tests at JLab in 2001 and 2002, crystal energy resolutions of $\frac{\sigma_E}{E} = 1.2\%$ and position resolutions of $\sigma_X = 1.2 mm$ were obtained for 4 GeV electrons[45], where the quoted value for position resolution is at the boundary between two lead tungstate crystal detectors. These results are consistent with those reported by the Mainz group for similar crystals operated at a stabilized temperature (8°C) where they attained:

$$\frac{\sigma_E}{E}(\%) = \frac{1.54}{\sqrt{E}} + 0.3, \tag{19}$$

with E given in GeV[46]. As compared to lead glass, use of these crystals will significantly

improve the radiation hardness of the detector near the beam line where radiation doses can be high. The central $12 \times 12 cm^2$ hole will be left open to enable the photon beam to pass through. The modules contiguous with this region on the beam axis as well as the two outermost layers of modules will be excluded from the fiducial volume of the detector to control coordinate resolution and detection efficiency near the boundaries of the detector. To monitor and correct possible gain changes due to temperature and aging, a light monitoring system will be used.

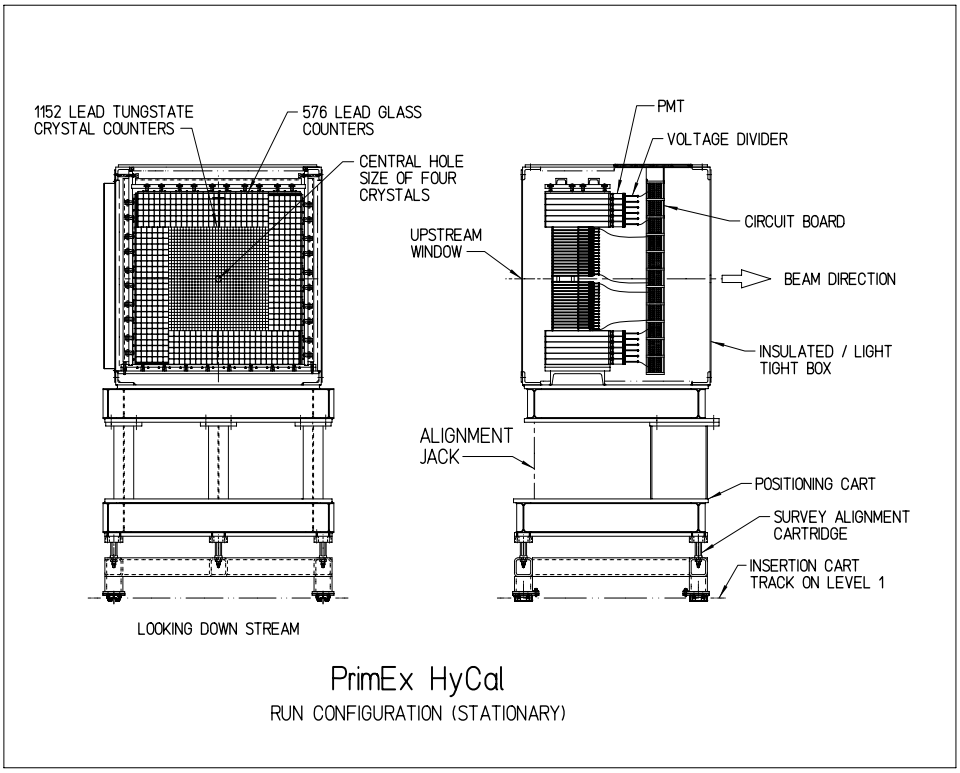

Figure 14: Schematic view of the HYCAL electromagnetic calorimeter with the transporter.

4.4 Rates and Uncertainties

In these experiments, the Primakoff amplitude will be extracted from the differential cross section measurements for the forward angle meson production. As mentioned earlier, the different angular dependence will enable identification of the Primakoff amplitude from the background nuclear coherent and interference contributions. We propose to perform a precision measurement of the differential cross sections on two different nuclei, ^1H and ^4He over a range of angles $(0-5^\circ)$ as determined by the electromagnetic calorimeter (see figure 15). The $1.5 \times 1.5 m^2$ calorimeter placed at a distance of $\sim 6m$ from the $10cm$ long liquid helium target will provide a high geometrical acceptance for the two decay photons, yielding detection efficiencies of $\sim 70\%$ (see figures 15 and 16). The expected experimental angular distribution

statistical	1.0% (60 days)
photon flux	2.0%
target thickness	1.5%
acceptance, misalignment	0.5%
Physics background	0.4%
beam energy	0.2%
nuclear coherent contrib.	1.0%
distorted form factor	0.3%
branching ratio	0.8% (PDB)
Total	3.1%

Table 1: Estimation of the experimental uncertainties for $\Gamma(\eta \to \gamma\gamma)$ measurement.

from a Monte Carlo simulation of $\eta \to \gamma\gamma$ events for a 30 day run is shown in figure 17. In this simulation, the experimental resolutions and all efficiencies of the setup are taken into account. The $\eta \to \gamma\gamma$ rate for a $10cm$ LHe4 target (1.3% r.l., $N(He^4) = 1.9 \times 10^{23} He^4/cm^2$) and 75 nA electron beam incident on a 10^{-4} r.l. bremsstrahlung Au target (5×10^7 equivalent photons/sec) is as follows:

$$\begin{aligned} N(exp.ev.) &= N(He4) \times N(gamma) \times (Int.CrossSec.) \times (eff.) \times (Br.Ratio) \\ &= 1.9 \times 10^{23} \times 5 \times 10^6 \times 1.6 \times 10^{-32} \times 0.7 \times 0.4 \\ &= 4.5 \times 10^{-3} (\eta \to \gamma\gamma)/sec \\ &= 400/day \\ &\sim 23,300 events/60 days \end{aligned} \tag{20}$$

Here we have taken the upper energy range of the tagged photon beam $\Delta E_\gamma = 1GeV$ only, for which $N_\gamma = 5 \times 10^6/sec$. The integral cross section over the angular range of 0-4 degrees for these energies is $\sim 1.6 \times 10^{-2}$ μbarns. The estimated experimental uncertainties for $\Gamma(\eta \to \gamma\gamma)$ are listed in table 1. The total error for the $\eta \to \gamma\gamma$ decay width has been estimated to be on the level of 3.1%, which includes 1.0% statistical error (for 60 days of beam time) and estimated systematic errors added in quadrature as shown in the table.

The $\eta' \to \gamma\gamma$ experiment has two major difficulties as compared with the the η decay width experiment. The first and most important one is that the $\eta' \to \gamma\gamma$ branching ratio is relatively small and poorly known. ($2.12 \pm 0.14\%$[16]). The branching ratio directly effects the number of events in the experiment, necessitating more beam time for this measurement. We estimate having $\sim 3.0\%$ statistical error for 90 days of beam time on a longer LHe4 target. The current error bar on the branching ratio ($\pm 6.6\%$) sets a lower limit on the total error of

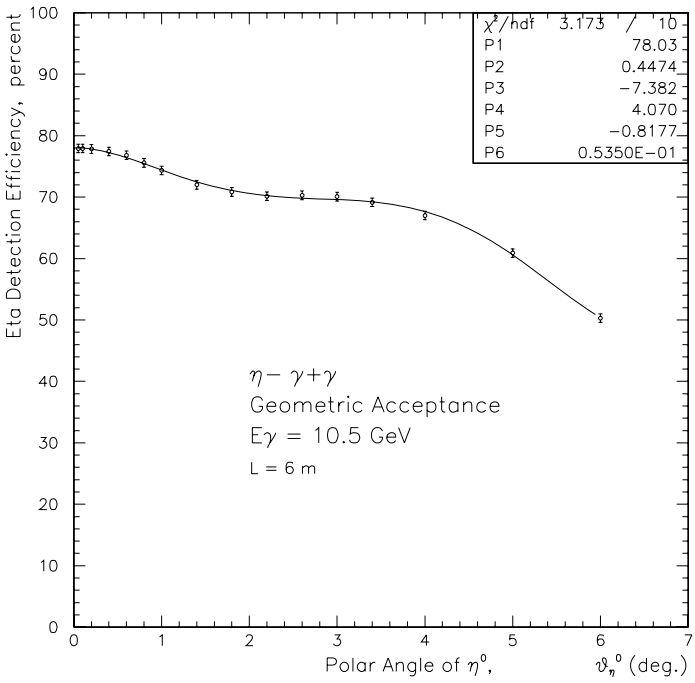

Figure 15: Geometrical acceptance of η's as a function of polar angle..

any new experiment. We expect this situation to be experimentally improved by the time we run the η' experiment. If this is not the case, we plan to run a dedicated experiment with a similar setup but, with an additional low momentum recoil detector. At the forward production angles (under the nuclear coherent part), the kinetic energy of the recoiling ^4He is in the range of 10-70 MeV as shown in figure 19. The produced η''s will be identified by recoil detection through missing mass reconstruction. At the same time, the decay photons will be detected by the downstream electromagnetic calorimeter. A preliminary conceptual design of the recoil detector includes a cylindrical multi-layer proportional chamber under $\sim$ 5 atm ^4He gas pressure. The range of α's in a 5 atm ^4He gas is shown in figure 20 as a function of kinetic energy. The differential cross section at the forward angles for the η' meson is shown in figure 18. Only the Primakoff contribution is shown here, since there are no experimental data for the η' done with the fix target technique. Our estimation is that with 90 days of beam time and using a 15 cm LHe4 target we can reach a 3.0% systematic error for the η' decay width measurement. The systematic errors are basically the same as for the eta experiment shown in the table 1, except for the branching ratio. Assuming that one can attain a $\sim$ 3.0% error in the knowlage of the branching ratio, we estimate the total error of the determination of the $\eta' \to \gamma\gamma$ decay width to be on the level of 5%.

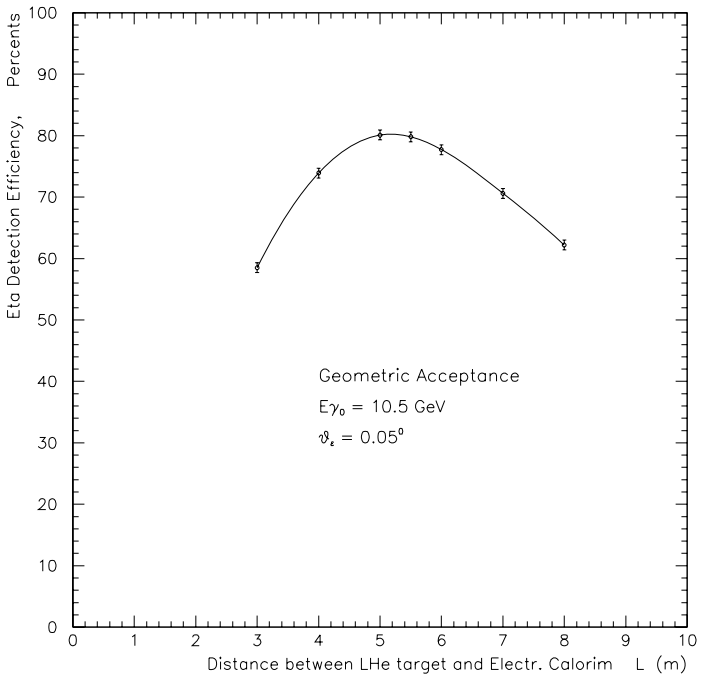

Figure 16: Geometrical acceptance of η's as a function of target to calorimeter distance.

5 Measurements of the Transition Form Factors $F_{\gamma\gamma^*P}$

Studies of the $\gamma\gamma^*P$ vertex, where P represents the π^o, η, or η' pseudoscalar mesons and γ^* is a virtual photon, enable one to study the transition regime from soft nonperturbative physics to the hard processes of perturbative QCD. We propose to measure the photon momentum dependence of the form factors $F_{\gamma\gamma^*P}(Q^2)$ and thereby map out an extension to the axial anomaly to provide a clean test of QCD predictions for exclusive processes.

The structure of the meson's electromagnetic coupling is typically parameterized in the context of the vector meson dominance model in which a photon couples to hadronic matter via an intermediate vector meson. Such a model implies a form factor of the form:

$$F_\pi = \frac{1}{1 + q_\mu^2/m_V}, \tag{21}$$

where m_V is the mass of the vector meson. For the charged pion case, the Coulomb form factor has been measured[47] and the charge radius was determined to be about 0.6 fm. Due to charge conjugation symmetry, however, the elastic Coulomb form factor (γPP) vanishes. The $\gamma^*\gamma P$ transition vertex, on the other hand, is of great interest and has been studied theoretically from the point of view of models based on the VMD as well as those involving treatments of the quark substructure [48][49][50][51][52][53][54][55][56] [57][57][58][59] . This

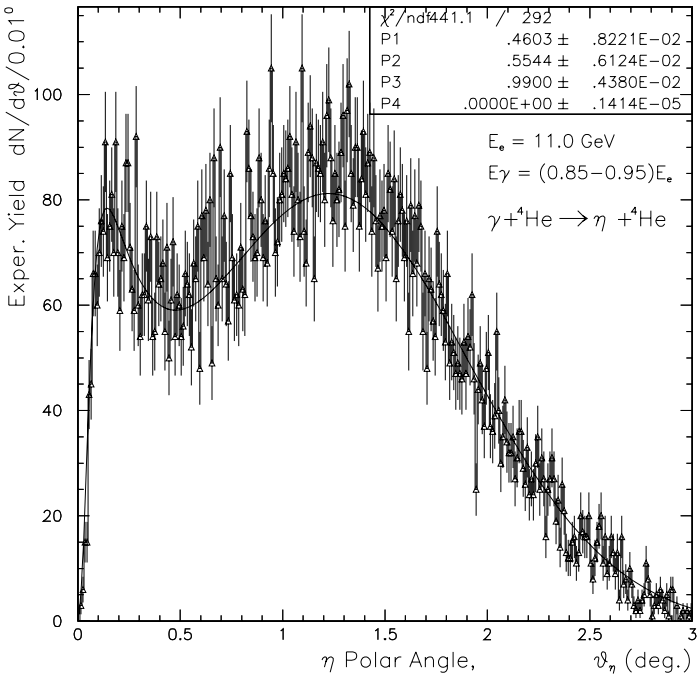

Figure 17: Monte Carlo simulation of expected yield as a function of angle for $\eta\gamma\gamma$ events on ^4He.

transition is characterized by the form factor $F(q_1^2, q_2^2)$ which, if only one photon is significantly off shell, depends upon a form factor typically parameterized by the pole form (9), and approximated at low q_μ^2 by:

$$F_{\gamma^*\gamma\pi^o} \approx 1 - a\frac{q_\mu^2}{m_P^2}. \tag{22}$$

where the slope a is a measure of the $\gamma^*\gamma P$ interaction radius. A determination of the slopes of the π^0, η and η' form factors would uniquely fix a low energy constant $\mathcal{O}(p^6)$ in the effective chiral Lagrangian[14].

The low, as well as high, Q^2 behavior of this form factor has been the source of considerable theoretical efforts. As pointed out in Bijnens [71], the next to leading order contributions are quite different when one of the photons is off shell. While the loop contributions tend to cancel when both photons are real, they have significant effect in the virtual case.

Despite the theoretical interest in pseudoscalar meson form factors, the experimental situation remains incomplete. Here, we indicate the experiments which have been performed, and the contributions which could be made with 11 GeV electron beams using the virtual Primakoff effect.

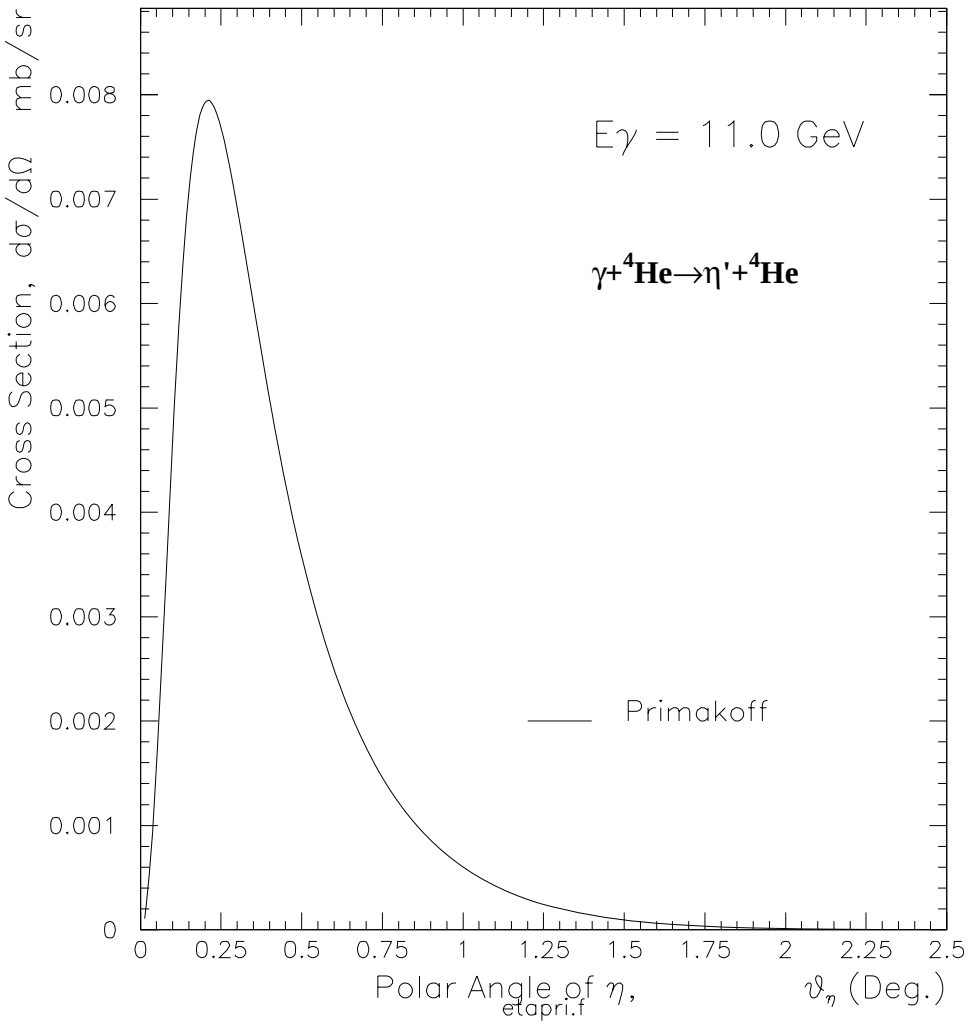

Figure 18: Coulomb photoproduction of η' as a function of angle.

5.1 Previous Measurements in the Space-like Region

A number of experiments have been performed to measure these transition form factors. However, existing data in the low and intermediate regions are quite poor. The CELLO collaboration at PETRA has measured $F_{\gamma^*\gamma P}$ in the space-like region at large momentum transfers using the reaction $e^+e^- \rightarrow e^+e^-P$[17]. In this experiment, two photons are radiated virtually by the colliding e^+e^- beams. One of the virtual photons is close to real and the other has a larger q_μ^2 and is tagged by the detection of an e^+ or e^-.

Measurements were taken at momentum transfers ranging from 0.62 to 2.17 $(GeV/c)^2$, and the value of a was deduced by extrapolation under the assumption of vector meson dominance. The authors quote values of $a_{\pi^0} = 0.0325 \pm 0.0026$, $a_\eta = 0.428 \pm 0.063$, and $a_{\eta'} = 1.46 \pm 0.16$. Only the statistical errors have been taken into account in these results with systematic errors estimated to be of the same order as the statistical error. The results of these measurements are shown in figure 21 for the π^o and 22 for the η^o with the corresponding fit to $F_{\gamma^*\gamma P}$. From the plots, it is clear that any extraction of the slope parameter at $Q^2 = 0$ using the experimental data at relatively large Q^2 is highly model dependent. Data covering the higher q_μ^2 region from 2 to 20 GeV^2 on these mesons have also been reported by the CLEO collaboration[72].

The low and intermediate momentum transfer region for these mesons is largely unexplored experimentally. While the L3 Collaboration has some results (with very poor Q^2 resolution) in the low Q^2 region for the η', low and intermediate Q^2 data on the π^o and η are totally lacking. The advent of 11 GeV electrons at JLab, however, will make such studies possible.

5.2 Previous Experiments in the Time-like Region

A number of experiments aimed at measuring a have been performed in the time-like momentum transfer region utilizing the π^o and η Dalitz decay $\pi^o/\eta \rightarrow e^+e^-\gamma$ reaction [60][61][62][63][64][65] [66][67][68][69]. The amplitude for this process involves the $F_{\gamma^*\gamma P}$ form factor which, in the usual linear expansion

$$F(x) \approx 1 + a\frac{m_{e^+e^-}^2}{m_P^2}. \tag{23}$$

A summary of these measurements on the pion is shown in the figure 23, where it can be seen that the published values for the slope range from -0.24 to $+0.12$. Such experiments suffer from small kinematically accessible ranges and significant backgrounds, and they require large final-state radiative corrections. As such, these experiments have not been able to determine even the sign of the form factor slope.

5.3 The Proposed Experiments

In 1989, Hadjimichael and Fallieros[70] suggested that the virtual Primakoff effect could access additional fundamental information about the pion, as the cross section is proportional

to $|F_{\gamma^*\gamma\pi^o}(q_\mu^2)|^2$. The full expression for the virtual Primakoff scattering cross section is[70]:

$$\frac{d^3\sigma}{d\epsilon_2 d\Omega_2 d\Omega_P} = \frac{Z^2\eta^2}{\pi}\sigma_M \frac{\vec{q}_p^{\,4}}{\vec{k}^4}\frac{\beta_P^{-1}}{\omega_P}|F_N(K^2)|^2|F_{\gamma^*\gamma P^o}(q_\mu^2)|^2 sin^2(\frac{\theta_e}{2})sin^2(\theta_P) \times[4\epsilon_1\epsilon_2 sin^2\phi_P + |\vec{q}|^2/cos^2(\frac{\theta_e}{2})] \quad (24)$$

where σ_M is the Mott cross section, $\eta^2 = (4/\pi m^3)/\tau$, τ is the meson lifetime, K is the (nearly real) photon four momentum from the Coulomb field, the meson four momentum is $Q = (\vec{q}_p, \omega_P)$, $\beta_p = \vec{q}_P/\omega_P$, and $F_N(K^2)$ is the nuclear charge form factor. This expression for the cross section in similar to that for the real Primakoff effect, with the notable exception of the form factor $|F_{\gamma^*\gamma P}(q_\mu^2)|^2$ which is of interest here.

Hadjimichael and Fallieros examined the sensitivity of the π^0 Primakoff cross section to a for energy transfers up to 1.6 GeV. They saw only moderate sensitivity and noted that the cross section is optimized for $\theta_e \to 0$ and $\theta_\pi \to 0$ whereas pion energies above 2 GeV are favored for probing the $\gamma^*\gamma\pi^o$ vertex. We have extended these calculations to kinematical ranges available with the proposed 11 GeV electron beam at JLab and note that good sensitivity to the $\gamma^*\gamma P$ form factor is present.

Figure 24 shows the cross sections for the virtual Primakoff pion photoproduction process on helium-4 as a function of $E_{e'}$, with an electron scattering angle of 2 degrees and a pion angle, $\theta_{\pi^o\vec{q}}$, of 0.1 degrees. The incident energy is 11 GeV. The two curves are for the VMD prediction ($a = 0.03$) and that using the slope parameter determined by the $\pi^o \to e^+e^-\gamma$ experiment ($a = 0.1$) of reference [65]. From the plot one can see that the cross sections are large, and are quite sensitive to the pion transition form factor.

5.3.1 Experimental Considerations

We argue that with minor modifications, one can use the previously discussed highly segmented calorimeter to perform measurements of the light pseudoscalar transition form factors in the very low Q^2 region. Photons from the decay of the π^o and η^o, as well as the scattered electrons, will be detected in the calorimeter. In the simulations discussed below, a 10 cm long liquid helium-4 target was assumed. The calorimeter is taken to be $1.5m \times 1.5m$ in size, with a $12cm \times 12cm$ central hole to allow the beam to pass through. (See figure 6.) Typical target to detector distances are about 6-8 meters. With such a setup, the resulting cross section weighted kinematical acceptances for π^o Primakoff production are those shown in figure 25.

In order to distinguish the Primakoff mechanism from other photoproduction processes, one must ascertain that the setup has sufficient resolution. Figure 26 shows the θ_π angular dependence of the cross section for pion photoproduction with the contributions from Primakoff, nuclear coherent, and their interference as indicated. It is this angular dependence which we plan to measure with the proposed highly segmented calorimeter in order to separate the photoproduction amplitudes. A Monte Carlo simulation of the effect of the target thickness and detector resolution on the reconstructed meson production angle is shown in figure 27. It can be seen that the $\theta_{\vec{q}P}$ resolution for target thicknesses up to 10 cm is sufficient to resolve the Primakoff peak.

The Q^2 acceptance is shown in figure 28, where the electron energy transfers are restricted to regions (ν between 8 and 10.5 GeV) where the virtual photon angle uncertainty is at a minimum. It can be seen that this setup complements the CELLO measurements in covering the extremely low Q^2 region ($Q^2 \sim 0.001$–0.5 GeV^2) which is unavailable to the collider experiments.

Figure 29 shows the resolutions in Q^2 and reconstructed η production angle with respect to the virtual photon direction at $Q^2 = 0.1GeV^2$ and $\theta_\eta = 0.1^o$ resulting from finite position and energy resolutions in the detection of the scattered electrons and two decay photons of the η in the calorimeter. Similar results are obtained for the π^o. It can be seen that the Q^2 and $\theta_{P\vec{q}}$ resolutions are more than adequate to extract the Q^2 dependence of $F_{\gamma\gamma^* P}$.

Figure 30 shows the calorimeter acceptance for Primakoff produced η's as a function of the z position of the detector with respect to the target. Six meters has been chosen to optimize the detector acceptance and resolution for η's. Due to its lower mass, the opening angle between the pion decay photons is typically lower and therefore one can tolerate a somewhat larger target to detector distance. There is good acceptance (75% to 95% at 9 GeV) for pions out to five degrees from the beamline for a target to detector distance of 7.5 m. This would enable good acceptance for pions produced via nuclear coherent photoproduction and therefore an accurate determination of background amplitudes.

With this experimental setup, we expect a yield of $\sim 1.0 \times 10^5$ π^o's and $\sim 2.0 \times 10^4$ η's per day for a $100nA$ electron beam current, where the branching ratio for two photon decay of the η was taken to be 39%. Anticipated results for a 30 day run are shown in figures 21 and 22.

6 Utilization of the Apparatus for Future Measurements

6.1 $\eta \to \pi^0\gamma\gamma$ Decay

The highly segmented electromagnetic calorimeter proposed here will be very efficient in detecting multi-photon final states. Another reaction of great interest which could be studied with such a setup is $\eta \to \pi^0\gamma\gamma$. This decay channel has a very long and dramatic history (which is nicely reviewed in Ref. [77]), and has attracted much attention from both theoretical and experimental points of view in the past three decades. In lowest order ChPT the tree level amplitudes vanish at both $\mathcal{O}(p^2)$ and $\mathcal{O}(p^4)$, and the first non-vanishing contribution comes from $\mathcal{O}(p^4)$ loop terms [78]. However, loops involving kaons are largely suppressed due to the kaon masses, while the pion loops are suppressed due to G parity. The first sizable contribution comes at $\mathcal{O}(p^6)$. Thus, this decay channel provides a unique probe for higher order corrections in ChPT. Because $\mathcal{O}(p^6)$ coefficients are not precisely determined, these effects cannot be calculated without model ambiguities. Some recent theoretical estimates are given in Table 2. A recent article indicates that the two-photon invariant mass spectra have different shapes for different mechanisms in the process as shown in figure 31. Experimental

Prediction	Reference	$\Gamma(\eta \to \pi^0\gamma\gamma)(eV)$
Ko ($\mathcal{O}(p^4)$)	[79]	0.004
Ko	[80]	0.47 ± 0.20
Ametller et al.	[78]	0.42 ± 0.20
Nemoto et al.	[81]	0.92
Bellucci and Bruno	[82]	0.58 ± 0.3
Ng and Peters (VMD)	[83]	$0.30^{+0.16}_{-0.13}$
Ng and Peter (Box)	[84]	0.70
E. Oset et al.	[85]	0.47 ± 0.10

Table 2: Theoretical predictions of the decay $\eta \to \pi^0\gamma\gamma$.

measurement of such spectra would be very desirable to resolve the model ambiguities.

About 20 experiments have been performed to measure this decay width since 1966. Despite considerable experimental effort, however, only one sufficiently sensitive result has been published (by GAMS-2000[86]):

$$\Gamma(\eta \to \pi^0\gamma\gamma) = 0.84 \pm 0.18eV, \tag{25}$$

which is about two times larger than all ChPT predictions. A recent report on the preliminary result of the CB experiment based on 500 events indicates that $\Gamma(\eta \to \pi^0\gamma\gamma) = 0.42 \pm 0.14$ eV[87], which is within the range of the theoretical predictions. Confirmation of this preliminary result and the measurement of the $\gamma\gamma$ invariant mass distribution should be a high priority.

The major challenge in this measurement is to suppress the background from $\eta \to 3\pi^0$. It imitates the desired $\eta \to \pi^0\gamma\gamma$ signature through the merging of photons in the photon detector[77]. The high granularity of the calorimeter described in this proposal will greatly help to discriminate merged photons in the detector by examining the energy deposition profile of the corresponding electromagnetic shower in the transverse direction. The new generation of calorimeter techniques using $PbWO_4$ crystals also ensures better angular and energy resolutions than those in any other experiment performed thus far. The JLab 12 GeV upgrade will increase the detector geometrical acceptance by boosting the photons to the forward direction, enabling the operation of the calorimeter at relatively higher threshold in order to reduce the background.

6.2 $\eta \to \pi^0\pi^0$

In recent years, searching for new physics beyond the Standard Model has become a prime task for physicists. A good place to search for new physics is to test the basic symmetries of charge conjugation (C), parity (P), and time reversal (T), as well as CP and CPT in the different interactions[88]. Since the discovery of a 0.2% CP violation in 1964 came as a great surprise, the origin of this violation remains the most mysterious phenomenon in elementary particle physics. CP violation is incorporated into the Standard Model by means of

complex coupling constants in the quark matrix and is controlled by a single parameter - the Kobayashi-Maskawa phase[89]. This violation shows up in family-changing interactions, while in family-conserving cases CP violation is observably small. The experimental verification of the second case is still very poor. The decay of $\eta \to \pi^0\pi^0$ is among four tests listed in the Review of Particle Physics[92] to study non-conventional CP violating effects. Since $\eta \to \pi^0\pi^0$ is a flavor-conserving interaction, the expected branching ratio in the Standard Model is small. A recent calculation indicates that $BR(\eta \to \pi^0\pi^0)$ should be less than 3×10^{-17} [91]. The current experimental limit on the 2π decay of the η is[92]:

$$BR(\eta \to \pi^0\pi^0) < 4.3 \times 10^{-4}. \tag{26}$$

The discovery of a much larger decay rate would be a sign for the existence of a non-conventional CP violation mechanism. We can improve the upper limit of $\eta \to \pi^0\pi^0$ as a by-product of an $\eta \to \pi^0\gamma\gamma$ measurement.

7 Summary

We have described a comprehensive program to measure the two photon widths and transition form factors of the pseudoscalar mesons (π^0, η, η') which would be possible with the advent of 12 GeV CW electron beams at Jefferson Lab. Precise measurements of these quantities will have a significant impact in the experimental determination of certain fundamental parameters of QCD, namely the light quark masses (m_u, m_d, m_s) and on the magnitude of $\eta, \eta^{'}$ mixing. At a more general level, these measurements impact the issue of spontaneous chiral symmetry breaking in QCD, and the intriguing question of whether the $\eta^{'}$ meson can be considered as a Goldstone Boson in the combined chiral and large N_c limits.

The proposed measurements of the π^0, η and η' transition form factors at very low Q^2 ($\sim$ 0.001–0.5GeV^2) would provide a first measurement of these important quantities. Physically, these can be approximately thought of as measuring the spatial distribution of the axial anomaly for each of the mesons. A determination of the slope of the π^o and η form factors would allow one to uniquely fix a low energy constant $\mathcal{O}(p^6)$ in the effective chiral Lagrangian[14] [4]. With a measurement of the η' form factor slope, one could also have a clear test of how good the U(3) flavor symmetry, implied by the large N_c limit holds. In this limit, the same low energy term determines all three transition form factor slopes. In addition, one important reason to better understand the transition form factors of the π^0, η and η' is that pseudoscalar exchange is the major contribution to the hadronic light-by-light scattering part of the muon anomalous magnetic moment[7]. It is thus important for future measurements of a_μ that search for "new physics" beyond the Standard model.

We believe the proposed instrumentation to be constructed for this program will be of general use to both this program, and future precision experiments, and will provide a new and powerful experimental window on QCD at JLab in an arena where the basic theory has been reasonably well developed.

8 Appendix I – The significance of the transition form factors for g-2

Contributed by Bing-An Li, University of Kentucky

We have proposed a measurement of the transition form factors $F_{\gamma\gamma^*P}$, in which one photon is real and the second is virtual. These, along with the analogous form factors in which both photons are virtual, are of considerable significance in ongoing searches for new physics beyond the Standard Model.

The Muon (g-2) Collaboration[1,2] has reported two new results for the anomalous magnetic moment of the muon:

$$a_\mu(exp.) = 11659202.3(15.1) \times 10^{-10}[1.3ppm] \text{ [93]},$$

$$a_\mu(exp.) = 11659204(7)(5) \times 10^{-10}[0.7ppm] \text{ [94]}.$$

The present world average is

$$a_\mu(exp.) = 11659203(8) \times 10^{-10}[0.7ppm].$$

The precision of these measurements permits a stringent test of the Standard Model, and a search for physics beyond it. For the time being, the SM's results are[95]

$$a_\mu^{SM} = \begin{cases} (11659168.5 \pm 8.1) \times 10^{-10} & [e^+e^- \text{ -based}] \\ (11659185.5 \pm 7.4) \times 10^{-10} & [\tau \text{ -based}] \end{cases}$$

Comparing with the data mentioned above, we have[3]

$$a_\mu^{exp} - a_\mu^{SM} = (34.5 \pm 11.4) \times 10^{-10} \quad 3.0\sigma discrepancy[e^+e^- based]$$

where the difference between the precision measurements and the SM is shown. However before any conclusion can be drawn, it is necessary to have a reliable standard model study[3]. The QED and weak contributions to a_μ have been calculated to high accuracy. A lot of work has been done on the hadronic contributions[3]. Nevertheless, there are still significant uncertainties. The major uncertainty is the contribution of the light-by-light scattering. While the contribution of the hadronic vacuum polarization is determined by the data from $\sigma(e^+e^- \to hadrons)$, determination of the contribution of light-by-light scattering depends on models[96] and is specified by the single and double transition form factors $F_{\gamma\gamma^*P}$ and $F_{\gamma^*\gamma^*P}$, where $P = \pi^0, \eta, \eta'$. The general expression for the double transition form factor is

$$F_{P\gamma^*\gamma^*}(q_1^2, q_2^2) = \sum_{ij} \frac{c_{ij}(q_1^2, q_2^2)}{(q_1^2 - m_i^2)(q_2^2 - m_j^2)}, \tag{27}$$

where m_i^2 is the mass of the i^{th} vector meson. In reference [97] the authors analyze the differences between the contributions of four different double transition form factors to the muon g-2.

The experimental situation is largely unexplored. Measurements of the branching ratio using $\pi^0 \to 2e^+ + 2e^-$ were performed in 1961 [68]. In this experiment 146 events are used to analyze the spin and parity of π^0 and the branching ratio was determined to be

$$B = (3.18 \pm 0.30) \times 10^{-5}.$$

So far there is no measurement of the form factor $F_{\pi^0}(q_1^2, q_2^2)$. For $\eta \to 2e^+ + 2e^-$, the only data is $B < 6.9 \times 10^{-5}$ [98].

The single transition form factors for pseudoscalars, the measurements of which have been described in this proposal, are also important contributors to the muon g-2. The contribution of light-by-light scattering to muon g-2 is expressed as

$$a^{Pl.b.l} = \int_0^{cut1} dq_1^2 \int^{cut2} dq_2^2 W(q_1^2, q_2^2) H(q_1^2, q_2^2), \tag{28}$$

where W is the well known kernel and H is a convolution of the single and double transition form factors. A further significance of the single transition form factors involves the determination of $c_{ij}(q_1^2, q_2^2)$ in equation 27. Most calculations arbitrarily take $c_{ij} = 1$, whereas the single transition form factor measurements will test this assumption.

In summary,

- Light-by-light scattering, (and therefore the pseudoscalar transition form factors), is the major uncertainty in the determination of muon g-2.
- The single transition form factors at low momentum transfers are currently extrapolated from CELLO data taken at high q^2 in a model dependent manner.
- No experimental data for the double transition form factors presently exist.

As such, it is our belief that *any* experimental input on the pseudoscalar transition form factors at low momentum transfer is of major significance in this Standard Model test.

References

[1] Report of the Special PAC 18 Review of the Science Driving the 12 GeV Upgrade.

[2] M. Gell-Mann, R. J. Oakes, and B. Renner. Phys. Rev. 175 (1968) 2195.

[3] J. L. Goity, A. M. Bernstein and B. R. Holstein, Phys. Rev. D66 (2002) 076014.

[4] B. Moussallam, Phys. Rev. **D51** (1995) 4939.
B. Ananthanarayan and B. Moussallam, hep-ph/02052702.

[5] P. Herrera-Siklódy, J. I. Latorre, P. Pascual and J. Taron, Nucl. Phys. **B497** (1997) 345, and Phys. Lett. **B419** (1998) 326.

[6] Johan Bijnens and Jürg Gasser, Proceeding for the workshop on eta physics, Uppasala, October 25-27, 2001

[7] Andrzej Czarneki and William J. Marciano, Phys. Rev. D64, (2001), 013014.

[8] R. Kaiser and H. Leutwyler, in Non-perturbative Methods in Quantum, Field Theory, A. Schreiber, A. G. Williams and A. W. Thomas, Editors, World Scientific (Singapore 1998), hep-ph/9806336.
R. Kaiser and H. Leutwyler, Eur. Phys. J. **C17** (2000) 623.

[9] Th. Feldmann and P. Kroll, Eur. Phys. J. **C5** (1998) 327.
Th. Feldmann, P. Kroll and B. Stech, Phys. Rev. **D58** (1998) 114006.

[10] A. V. Anisovich and H. Leutwyler, Phys. Lett. B375 (1996) 335.

[11] Phys. Lett. B374 (1996) 181.

[12] F. Anulli, et al., p. 607 in Vol. II of The second $DA\Phi NE$.

[13] A. Browman et al., Phys. Rev. Letts., vol. 33, no. 23, (1974)1400.

[14] J. Bijnens, A. Bramon and F. Cornet, Phys. Rev. Lett. 61 (1988) 1453.

[15] E.P. Venugopal and B.R. Holstein, Phys. Rev D57 (1998) 4397.

[16] D. Haidt et al edit, Review of Particle Physics, Vol 3, (1998).

[17] H.J. Behrend, et, al., Z. Phys. C, 49 (1991) 401.

[18] M. Acciarri et al., Phys. Lett. B418 (1998) 399.

[19] J.F. Donoghue, E. Golowich, and B.R. Holstein, Dynamics of the Standard Model, Cambridge University Press (1992).

[20] J.S. Bell and R. Jaciw, Nuovo Cimento 60A (1969) 47; S.L. Adler, Phys. Rev. 177 (1969) 2426.

[21] International workshop on the structure of the η' meson, March 8–9, 1996, edited by M. Burkardt, J. Goity, V. Papavassiliou and S. Pate, World scientific.

[22] R. Baur, J. Kambor and D. Wyler, Nucl. Phys. B460 (1996) 127.

[23] J. F. Donoghue, B. R. Holstein and Y. C. R. Lin, Phys. Rev. Lett. 55 (1985) 2766.

[24] J. Gasser and H. Leutwyler, Nucl. Phys. B250 (1985) 465.

[25] Hall D PCDR.

[26] V.V. Anisovich et al, Phys.Lett.B404(1997)166.

[27] G. Bellettini et al., Il Nuovo Cimento, vol. 66, no. 1, (1970), 243.

[28] C.E. Hyde-Wright, W.Bertozzi and J.M. Finn, In Newport News 1985, Processdings, Continuous Electron Beam Accelerator Facility 532-551.

[29] R. Wilson, lecture given at Scottish University Summer School, T.W. Priest and L.L.J. Vick edit, Oliver and Boyd,1966.

[30] C.A. Engelbercht, Phys., Rev., 133, B988 (1964).

[31] N.A. Roe, Particle Data Book, 1994.

[32] M. Vanderhaeghen, M. Guidal, and J.-M. Laget, Phys.Rev.C 57, 1454 (1998).

[33] M. Branschweig, et al., DESY preprint, 70/1.

[34] A. Breskin, G. Charpak, S. Majewski, Nucl. Instr. and Meth. 220 (1984)349.

[35] K. Assamagan et al., Nucl. Instr. and Meth. A426(1999)405.

[36] K. Pysz et al., Nucl. Instr. and Meth. A420 (1999) 356

[37] J. Drexler et al., Nucl. Instr. and Meth. 220 (1984) 409

[38] E.A. Arakelyan et al., Physics of Atomic Nuclei, v.58, n2(1995)219

[39] M. Overbeck et al., Nucl. Instr. and Meth. A288 (1990) 413

[40] M. J. M. van Sambeek et al., Nucl. Phys. A631 (1998) 545c

[41] M. J. M. van Sambeek et al., Nucl. Instr. and Meth. A434 (1999) 279.

[42] C. B. Fulmer, B.L. Cohen, Phys.Rev.,109 (1958) 94.

[43] P. Armbruster et al., Nucl. Instr. and Meth. 91(1971)499.

[44] Michael PAUL et al., Nucl. Instr. and Meth., A277 (1989) 418.

[45] Ashot Gasparian, Proceeding of the 10th international conference on the calorimeter, Pasadana, 2002.

[46] K. Mengel, R. Novotny, R. Beck, *et al.*, "Detection of Monochromatic Photons Between 50 and 790 MeV with a $PbWO_4$ - Scintillator Array", to be published (1999).

[47] S.R. Amendolia et al., Phys. Lett. 146B (1984) 116.

[48] L.G. Landsberg, Phys. Rep. 128, no. 6 (1985) 302.

[49] P. Maris, nucl-th/0008048, 24 Aug 2000.

[50] B.-A. Li, hep-phy0102250, 20 Feb 2001.

[51] V.V. Anisovich, et al., hep-ph/9702383, 21 Feb 1997.

[52] V.V. Anisovich, et al., Phys. Rev. D, 55, number 5, (1997) 2918.

[53] P. Maris, P.C. Tandy, Nucl. Phys A663 (2000), 401c.

[54] P. Tandy, Fizika B, (1999),295.

[55] C.D. Roberts, Nucl. Phys A 605 (1996), 475.

[56] M.R. Frank, K.L. Mitchell, C.D. Roberts, P.C. Tandy, Phys. Lett B 359 (1995) 17.

[57] M.A. Ivanov and V.M. Shekhter, Sov. J. Nucl. Phys 32(3) (1980), 410.

[58] H. Ito, W.W. Buck, F. Gross, Phys. Lett. B 287 (1992) 23.

[59] I.V. Musatov and A.V. Radyushkin, Phys. Rev. D, volume 56, number 5 (1997), 2713.

[60] R. Meijer Drees et al. Phys. Rev. D, Vol 45, no 5 (1992) 1439.

[61] F. Farzanpay et al., Phys. Lett. B278 (1992) 413.

[62] H. Fonvieille et al., Phys. Lett. B233 (1989) 65.

[63] P. Gumplinger, Doct. Thesis, Oregon State University (1987); J.M. Poutissou et al., Proc. Lake Louise Winter Institute (1987), World Scientific, Singapore.

[64] G. Tupper et al., Phys. Rev. D28, no 11 (1983) 2905.

[65] J. Fischer et al., Phys. Lett., Vol 73B, no. 3 (1978) 359.

[66] J. Burger, Doct. Thesis, Columbia University (1972).

[67] S. Devons et al., Phys. Rev., vol. 184, no. 5 (1969) 1356.

[68] N.P. Samios, Phys. Rev. Vol 121, no 1 (1961) 275.

[69] H. Kobrak, IL Nuovo Cimento, vol 20, no 6 (1961) 1115.

[70] E. Hadjimichael and S. Fallieros, Phys. Rev. C, vol. 39, no. 4 (1989) 1438.

[71] J. Bijnens, A. Bramon, F. Cornet, Z. Phys. C, 46 (1990) 599.

[72] D.M. Asner et al., CLEO CONF95-24, EPS0188, 1995

[73] D. Babusci et al., Phys. Lett. B 277, 158 (1992).

[74] M. Boglione and M.R. Pennington, Eur. Phys. J. C9 (1999) 11.

[75] J. Donoghue and B. Holstein, Phys. Rev. D, 48 (1993) 137.

[76] M. R. Pennington, "Riddle of the Scalars: Where is the σ?", unpublished.

[77] M.N. Achasov, et al., Nucl. Phys. B600, 3 (2001).

[78] L. Ametller, J. Bijnens, A. Bramon and F. Cornet, Phys. Lett. B276, 185 (1992).

[79] P. Ko, Phys. lLett. B349, 555 (1995).

[80] P. Ko, Phys. Rev. D47, 3933 (1993).

[81] Y. Nemoto et al., Phys Rev. D54, 6777 (1996).

[82] S. Bellucci and C. Bruno, Nucl. Phys. B452, 626 (1995)

[83] J.N. Ng and D.J. Peters, Phys. Rev. D46, 5034 (1992).

[84] J.N. Ng and D.J. Peters, Phys. Rev. D47, 4939 (1993).

[85] E. Oset, J.R. Pelaez, L. Roca, hep-ph/0210282, 2002.

[86] D. Alde et al., Yad. Fiz 40, 1447 (1984); D. Alde et al., Z. phys. C25, 225 (1984).

[87] S. Prakhov, UCLA Crystal Ball Report, CB-01-008.

[88] B.M.K. Nefkens and J.W. Price, Eta Physics Handbook, Workshop on Eta Physics, Uppsala 2001.

[89] T.D. Lee and C.N. Yang, Phys, Rev. 104, 254 (1956); Z.K. Silagadze, Phys. At. Nucl. 60, 272 (1997)

[90] D.E. Groom et al., Eur Phys. J., C15, 1 (2000).

[91] E. Shabalin, Eta Physics Handbook, Workshop on Eta Physics, Uppsala 2001; C. Jarlskog and E. Shabalin, Phys. Rev. D52, 248 (1995); C. Jarlskog and E. Shabalin, Phys. Rev. D52, 6327 (1995).

[92] Particle Data Book, Phys. Rev., D66, (2002)

[93] H.N.Brown et al.,Muon(g-2)Collaboration, Phys.Rev.Lett. **86**,2227(2001).

[94] G.W.Bennet et al.,Muon(g-2)Collaboration, Phys.Rev.Lett. **86**,2227(2001).

[95] see review articles: W.Marciano and B.Roberts, hep-ph/0105056; E. de Rafael, hep-ph/0208251.

[96] Hayakawa, T. Kinoshita and A. I. Sanda, Phys.Rev.Lett., **75**,790(1995), Phys.Rev.,**D54**,3137(1996); J.Bijnens, E.Pallante and J.Prades, Phys. Rev.Lett., **75**,1447(1995), Nucl.Phys.,**B474**,379(1996); M.Hayakawa and T.Kinoshita, Phys.Rev.,**D57**,465(1998), hep-ph/0112102; E.Rafael, hep-ph/0208251, references therein. M.Knecht, et al., Phys.Rev.Lett., **88**,071802(2002); M.Ramsey-Musolf and B.wise, Phys.Rev.Lett., **89**, 041601(2002).

[97] J. Bijnens and F. Persson, hep=ph/0106130.

[98] R.R.Akhmetshin et al., Phys. Lett., **B501**, 191(2001).

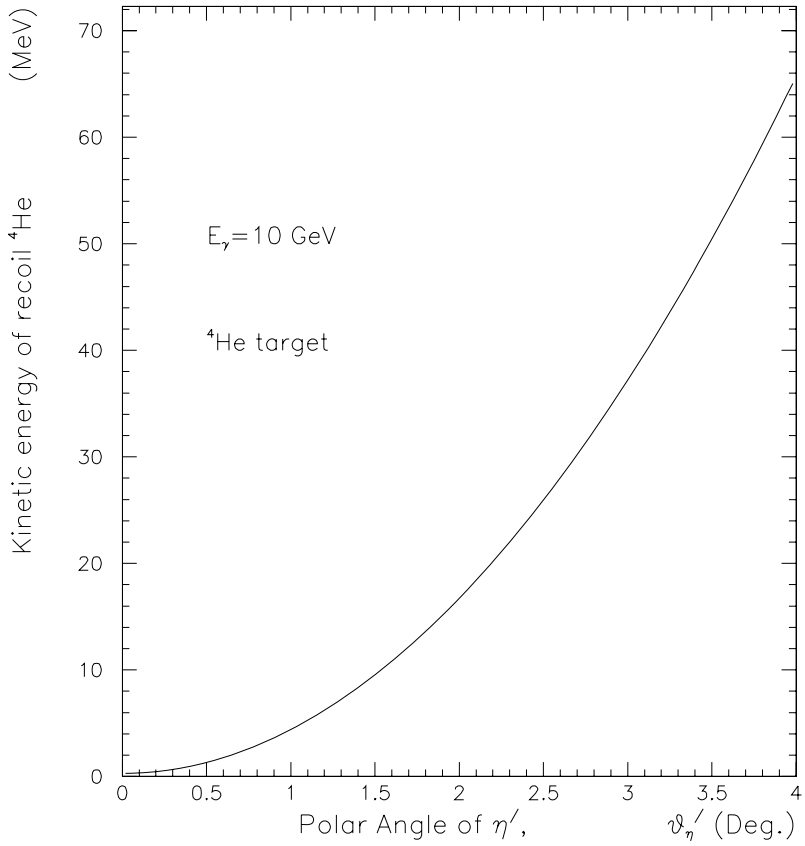

Figure 19: Kinetic energy of recoil ^{4}He from η' the production reaction.

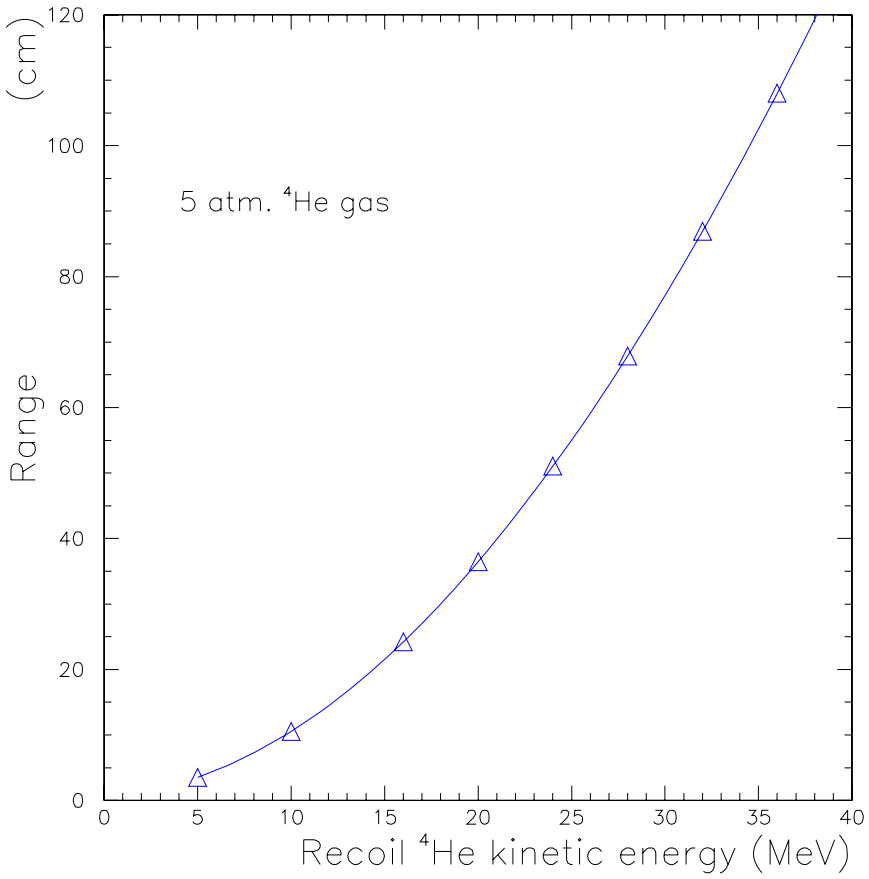

Figure 20: Range of recoil ^{4}He in ^{4}He gas for different kinetic energies.

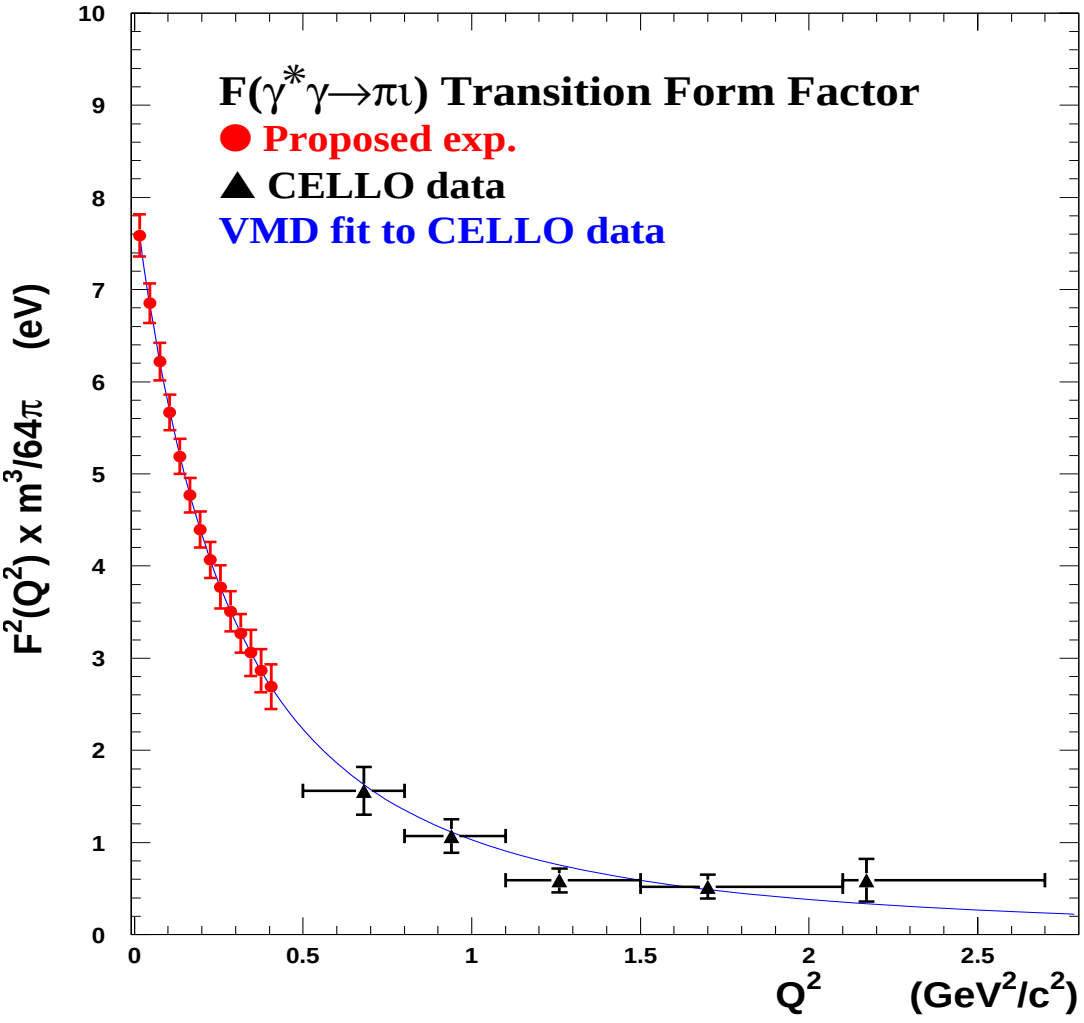

Figure 21: The π^o transition form factor. The proposed points are projected to the VMD prediction with expected total errors. CELLO data are from reference[17].

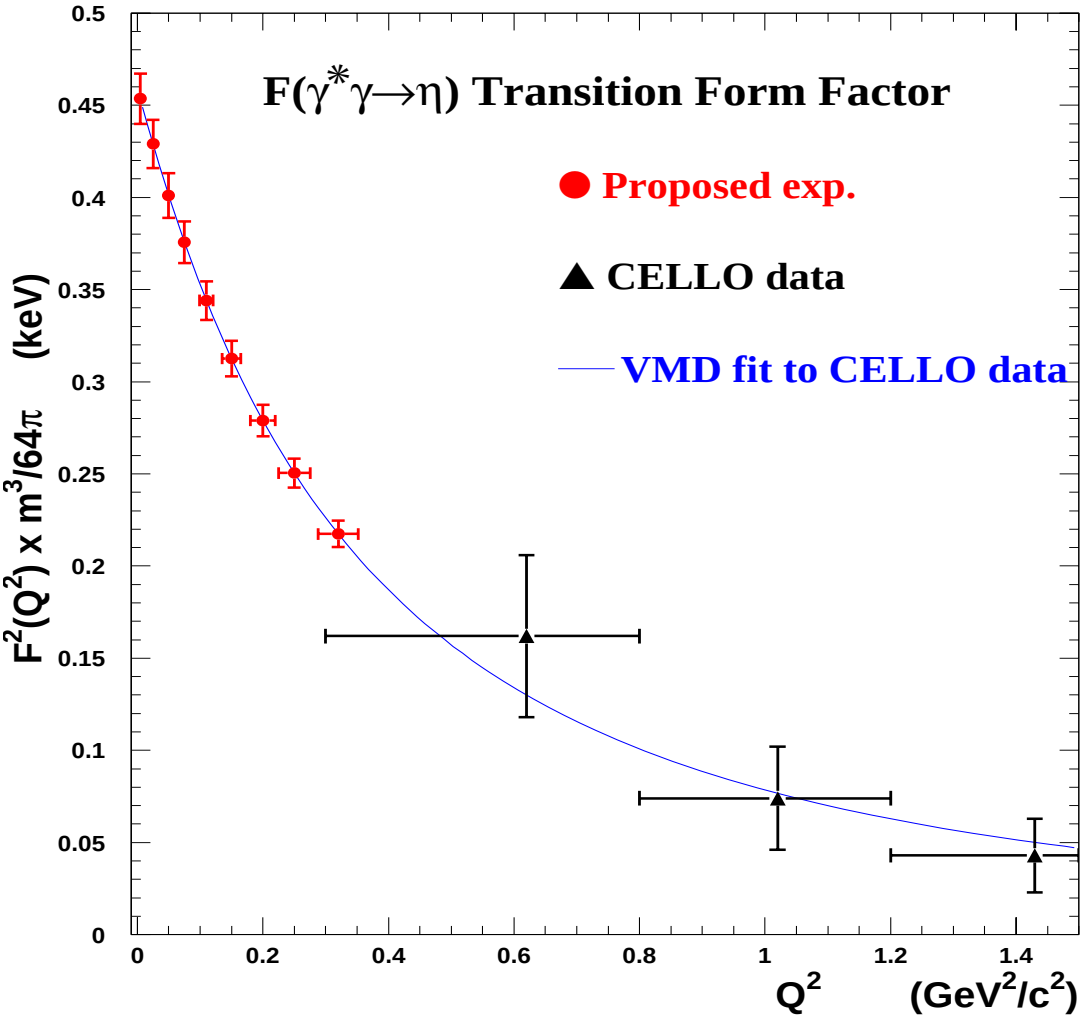

Figure 22: The η transition form factor. The proposed points are projected to the VMD prediction with expected total errors, in comparison with CELLO data[17].

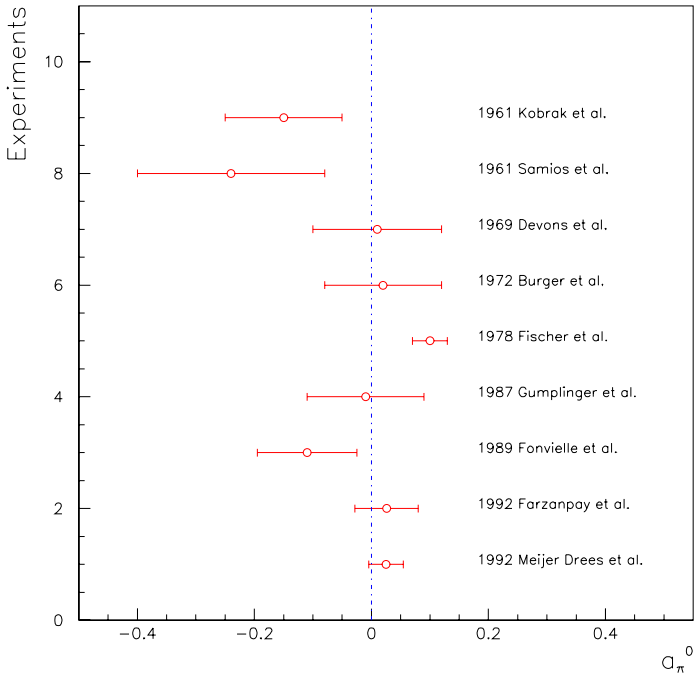

Figure 23: Summary of the previous slope measurements for the π^0 in the time-like region.

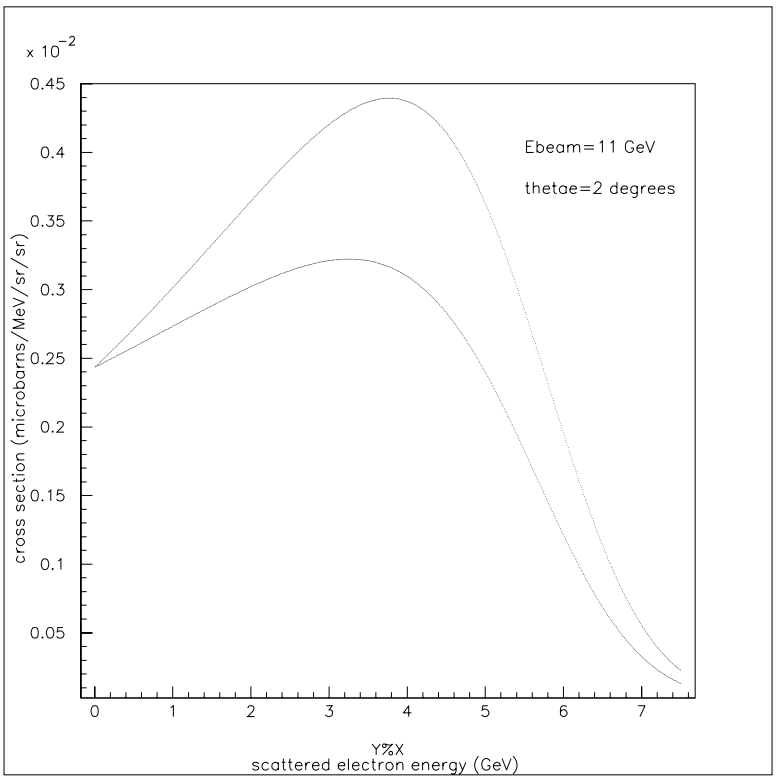

Figure 24: Cross section *versus* scattered electron energy for π^o production on helium-4. The incident electron energy is 11 GeV.

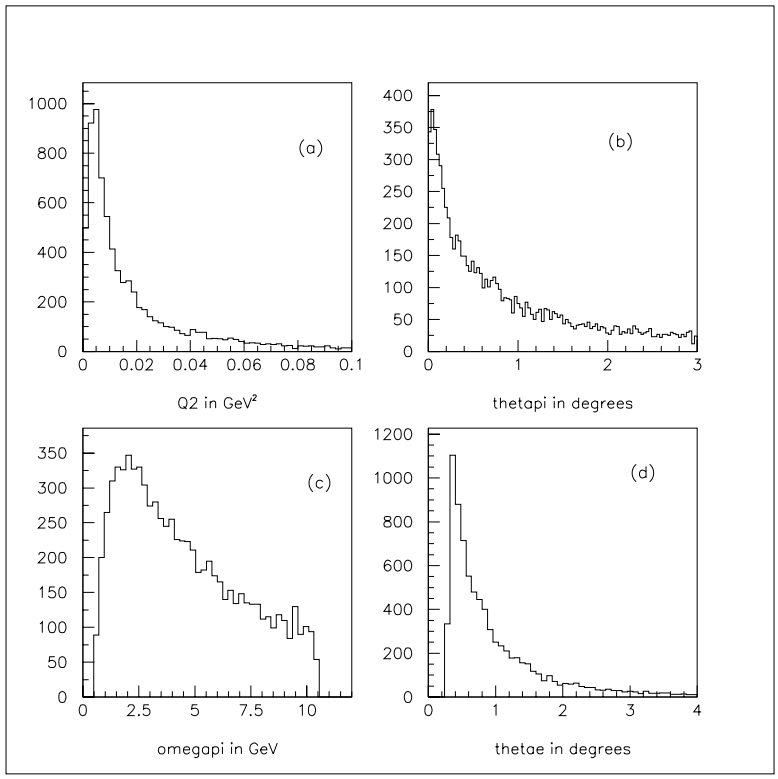

Figure 25: Primakoff pion production cross section weighted acceptances. (a) Q^2, (b) $\theta_{\pi\vec{q}}$, (c) ω_π, (d) θ_e. Target to detector distance is 7.5 m and central hole in calorimeter is $12cm \times 12cm$.

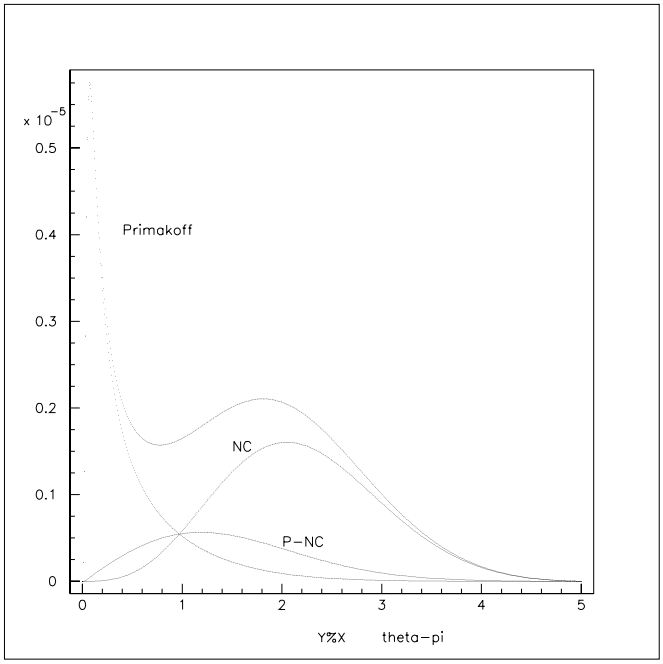

Figure 26: Cross section *versus* θ_π weighted by $sin(\theta_\pi)$ showing Primakoff, nuclear coherent, and their interference. In the plot, $E_e = 11GeV$, $\omega_\pi = 7GeV$, $\theta_e = 2^\circ$.

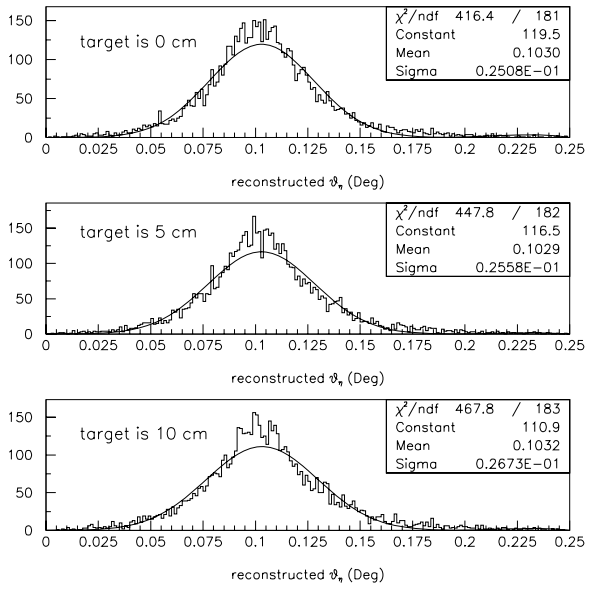

Figure 27: Reconstructed η production angle, $\theta_{\vec{q}\eta}$, at 0.1^o for three different target thicknesses. The distance between the target and the detector is 6 meters. Energy transfer is from 8 to 10.5 GeV, and Q^2 coverage is between 0.001 and 0.4 GeV^2.

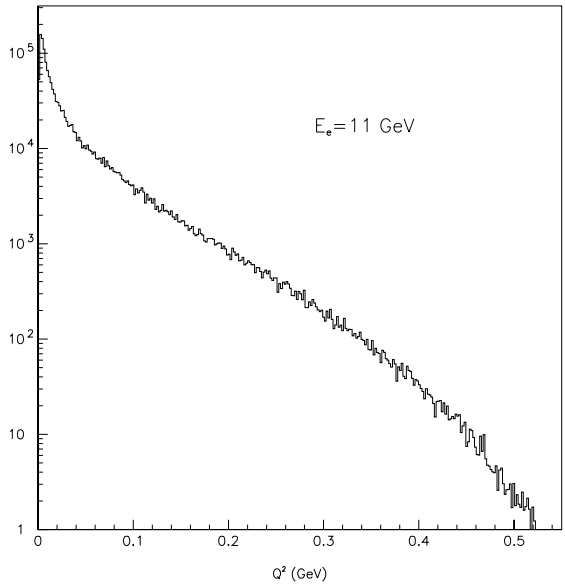

Figure 28: Monte Carlo simulation of Q^2 acceptance of a $1.5m \times 1.5m$ detector with a $12cm \times 12cm$ central hole. Detector is 6 m from target. Energy transfer is between 8 and 10.5 GeV.

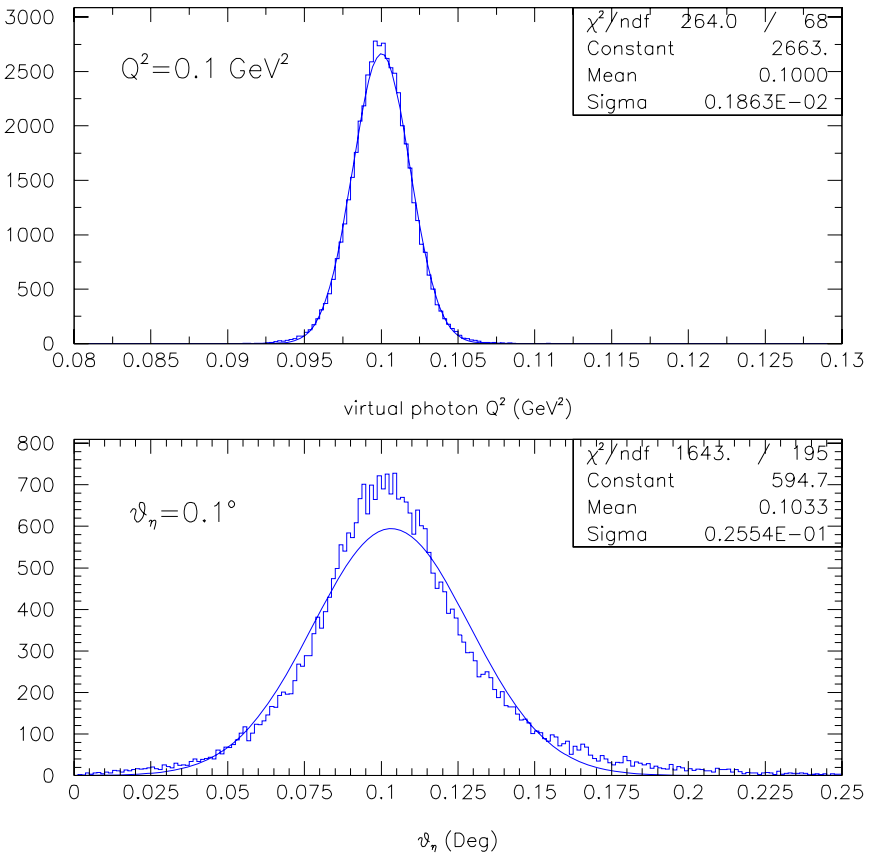

Figure 29: Monte Carlo simulations for actual reconstructed Q^2 resolution (top), and η production angle (bottom) for $Q^2 = 0.1GeV^2$, $\theta_\eta = 0.1^o$.

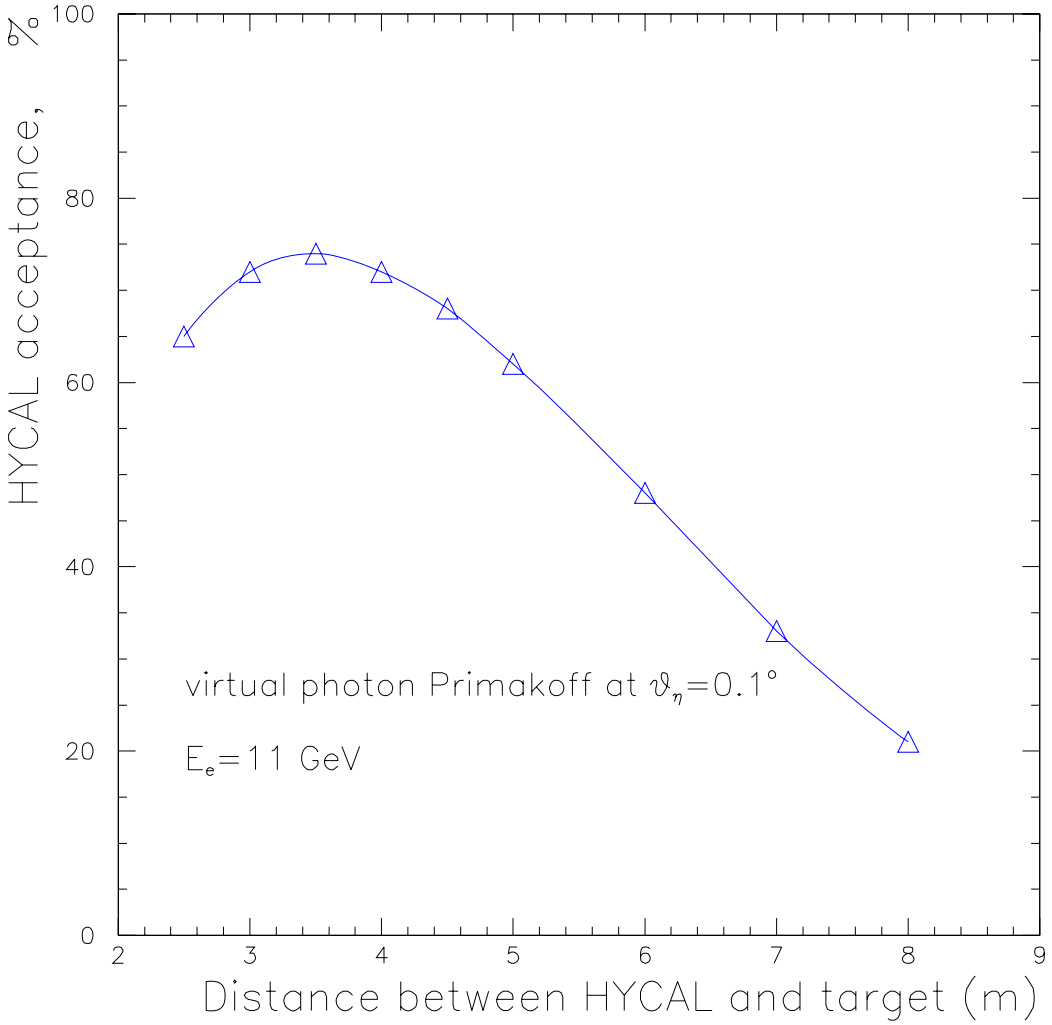

Figure 30: Calorimeter acceptance as a function of the distance between the target and the detector for the η production angle at 0.1^o. Energy transfer is from 8 to 10.5 GeV, and Q^2 coverage is between 0.001 and 0.4 GeV^2.

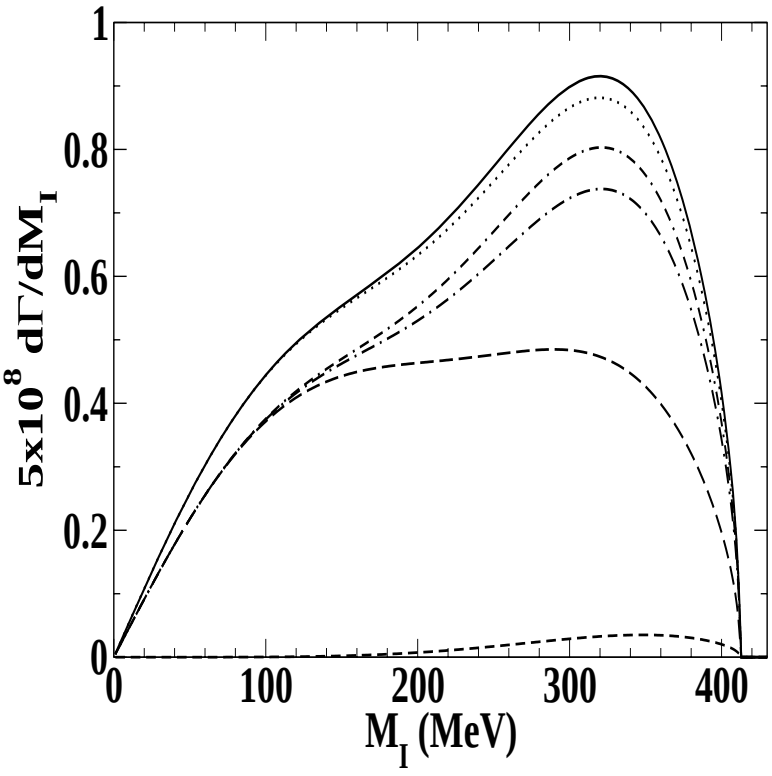

Figure 31: Different contributions to the invariant mass distribution of the two photons. From bottom to top, (1)short dashed line: only chiral loops; (2)long dashed line: only VMD tree level terms; (3)dashed-dotted line: coherent sum of the above two mechanisms; (4)double dashed-dotted line: idem but adding loop diagrams for VMD terms; (5)continuous line: idem but adding also the anomalous terms of involving $\gamma \to 3M$ vertex, which is the full model presented in this work. (6)dotted line, the full model but substituting the full $t_{K^+K^-,\eta\pi^0}$ scattering matrix by its lowest order $O(p^2)$). Figure is taken from Ref. [85].